Article:
Harvey, J, König, S and Luguet, A (2015) The effects of melt depletion and metasomatism on highly siderophile and strongly chalcophile elements: S–Se–Te–Re–PGE systematics of peridotite xenoliths from Kilbourne Hole, New Mexico. Geochimica et Cosmochimica Acta, 166. 210 - 233. ISSN 1872-9533

https://doi.org/10.1016/j.gca.2015.06.028

The effects of melt depletion and metasomatism on highly siderophile and strongly chalcophile elements: S-Se-Te-Re-PGE systematics of peridotite xenoliths from Kilbourne Hole, New Mexico.

Jason Harvey[1*], Stephan König[2], Ambre Luguet[3].

[1] School of Earth and Environment, University of Leeds, Leeds LS2 9JT, UK.
[2] Department of Earth Sciences, Universität Tübingen, Tübingen Germany.
[3] Steinmann Institut für Geologie, Mineralogie und Paläontologie, Rheinische Friedrich-Wilhelms Universität Bonn, Poppelsdorfer Schloss, 53115 Bonn, Germany.

[*] corresponding author: email - feejh@leeds.ac.uk. Tel - +44 (0)113 343 6769

For submission to Geochimica et Cosmochimica Acta

Abstract

The composition of the Earth's upper mantle is a function of melt depletion and subsequent metasomatism; the latter obscuring many of the key characteristics of the former, and potentially making predictions of Primitive Upper Mantle (PUM) composition problematic. To date, estimates of PUM abundances of highly siderophile element (HSE = platinum group elements (PGE) and Re) and the strongly chalcophile elements Se and Te, have been the subject of less scrutiny than the lithophile elements. Critically, estimates of HSE and strongly chalcophile element abundances in PUM may have been derived by including a large number of metasomatized and refertilized samples whose HSE and chalcophile element abundances may not be representative of melt depletion alone.

Unravelling the effects of metasomatism on the S-Se-Te-HSE abundances in peridotite xenoliths from Kilbourne Hole, New Mexico, USA, potentially provides valuable insights into the abundances of HSE and strongly chalcophile element abundances in PUM. Superimposed upon the effects of melt depletion is the addition of metasomatic sulfide in approximately half of the xenoliths from this study, while the remaining half have lost sulfide to a late S-undersaturated melt. Despite these observations, the Kilbourne Hole peridotite xenoliths have HSE systematics that are, in general, indistinguishable from orogenic peridotites and peridotite xenoliths used for determination of PUM HSE abundances.

This study represents the first instance where Se-Te-HSE systematics in peridotite xenoliths are scrutinized in detail in order to test their usefulness for PUM estimates. Despite earlier studies attesting to the relative immobility of Se during supergene weathering, low S, Se, Os and Se/Te in peridotite xenoliths suggests that Se may be more mobile than originally thought, and for this reason, peridotite xenoliths may not be suitable for making predictions of the abundance of these elements in PUM. Removal of Se, in turn, lowers the Se/Te in

basalt-borne xenolithic peridotites to subchondritic values. This is in contrast to what has been recently reported in kimberlite-borne peridotite xenoliths. Moreover, Te added to melt depleted peridotite in metasomatic sulfide is more difficult to remove in a S-undersaturated melt than the HSE and Se due to the generation of micron-scale tellurides. The effects of these processes in orogenic peridotites and xenoliths, from which PUM abundances have been calculated, require further scrutiny before unequivocal Se-Te-Re-PGE values for PUM can be derived.

1. Introduction

Two main processes affect the composition of the Earth's upper mantle; varying degrees of melt depletion (e.g. Frey and Green, 1974; Jagoutz et al., 1979; Galer and O'Nions, 1989) and the range of secondary processes grouped together under the broad umbrella of "metasomatism" (Harte, 1983). These include refertilization, i.e., the precipitation of metasomatic clinopyroxene (e.g. Le Roux et al, 2007, 2008, 2009; Soustelle et al., 2009; van Acken et al., 2010a), the infiltration of silicate melts and related fluids (Roden et al., 1984; Menzies et al., 1987; Schiano and Clocchiatti, 1994; Schiano and Bourdon, 1999), interaction with carbonatitic melts (O'Reilly and Griffin, 1988; Yaxley et al., 1991; Dautria et al., 1992; Ionov et al.,1993; Rudnick et al., 1993; Griffin et al., 1996) and / or CO_2-rich fluids (Andersen et al., 1984; O'Reilly and Griffin, 1988), the percolation of kimberlite-like melts (e.g. Menzies and Wass, 1983), and the cryptic effects of mechanical mixing of depleted peridotite with evolved cumulates (e.g. Riches and Rogers, 2011). The effects of metasomatism on lithophile trace elements (e.g. rare earth elements (REE), high field strength elements (HFSE) and large ion lithophile elements (LILE)) in melt-depleted peridotites have been understood for decades (e.g. Blundy and Wood, 1994; Wood and Blundy, 2001). Residual mantle is particularly vulnerable to re-enrichment in the most incompatible trace elements because depleted peridotite has very low concentrations of REE, HFSE and LILE compared to any of the melts and fluids with which it may interact (Navon and Stolper, 1987; Bodinier et al., 1990). Similar investigations into the effects of metasomatism on highly siderophile and strongly chalcophile elements, such as the platinum group elements (PGE: Os, Ir, Rh, Ru, Pt, Pd), Re, S, Se and Te, are less numerous (e.g. Morgan, 1986; Morgan et al., 2001; Ackerman et al., 2009; Alard et al., 2011; Wang et al.,

2013; Wang and Becker, 2013; König et al., 2014, 2015a). As a result, our understanding of the behavior of these elements during mantle processes is less complete.

Unlike lithophile trace elements, which are controlled by major silicate and minor oxide phases comprising > 99.9 modal percent of the mantle, the highly siderophile element (HSE = platinum group elements, (i.e., PGE and Re) inventory of the mantle is controlled by accessory Cu-Fe-Ni sulfides, also referred to as base metal sulfides (BMS). Experimentally determined sulfide / silicate partition coefficients for HSE and chalcogens ($D^{sulfide/silicate}$) of up to 5×10^4 (Peach et al., 1994; Fleet et al., 1991, 1996, 1999; Mungall and Brenan, 2014) were complemented by early studies on separated minerals (Morgan and Baedecker, 1983; Hart and Ravizza, 1996; Pattou et al. 1996; Burton et al., 1999; Handler and Bennett, 1999; Alard et al., 2000), and confirmed by in-situ measurements of BMS grains in peridotites (Alard et al., 2000; Lorand and Alard, 2001; Luguet et al., 2001, 2004; Lorand et al., 2008). Sulfide melts have been implicated in the metasomatism of peridotite (e.g. Bockrath et al., 2004; Ballhaus et al., 2006; Holzheid, 2010). The high solubility of S in silicate melts and C-O-H-S-rich fluids (e.g. Schiano and Clocciatti, 1994) provides a mechanism for both the dissolution and precipitation of BMS along grain boundaries and in intergranular interstices, dissolution and remobilization of BMS during fluid / melt-induced recrystallization of peridotite, or inclusion in secondary minerals, for example metasomatic clinopyroxene. An additional complication is the tendency for Te, along with its affinity for BMS, to form minute Pt-Bi-tellurides (Luguet et al., 2004; Lorand et al., 2008; Lorand and Alard, 2010). As a result, metasomatic BMS is easily transported and deposited in the mantle, thus obscuring the effects of prior melt depletion. Therefore lithophile trace elements, HSE and strongly chalcophile element fingerprints of partial melting can be easily smudged by seemingly ubiquitous secondary processes, i.e., post melt depletion, albeit it to differing extents for different groups of elements.

This presents problems for the calculation of the HSE and chalcogen composition of the Primitive Upper Mantle (PUM; Meisel et al., 2001; Becker et al; 2006; Walker, 2009), which requires an understanding of the composition of the Earth's mantle before it experienced melt extraction. Unfortunately, the ubiquity of metasomatic overprints make this difficult to constrain unequivocally. Several studies over the last 25 years have concluded that the major and trace element composition of many peridotites can be affected by silicate melt migration (e.g., Bodinier and Godard, 2003; Zhang et al., 2004; Le Roux et al., 2007; Piccardo et al., 2007; Dick et al., 2010; Batanova et al., 2011) and that many fertile lherzolites are in fact depleted harzburgites that have been subsequently refertilized through reaction with silicate melt (e.g. Elthon, 1992; Müntener et al., 2004; Le Roux et al., 2007, 2008, 2009; Soustelle et al., 2009). Similar processes may also affect the distribution of the HSE and chalcophile elements in mantle peridotites. For example, Cu-Ni-rich BMS precipitated on grain boundaries in peridotites are often enriched in Pd, Re, chalcogens and may possess radiogenic $^{187}Os/^{188}Os$ (e.g., Alard et al., 2000, 2002, 2005; Luguet et al., 2001; Pearson et al., 2004; Harvey et al., 2010, 2011). Co-precipitation of these interstitial sulfides occurs with the crystallization of clinopyroxene and spinel from silicate melts, i.e., lithophile, siderophile and chalcophile elements may all be affected by the interaction of melt-depleted peridotite with a silicate melt, but the degree to which melt depletion signatures are affected in each group of elements may vary considerably. In particular, the degree to which HSE and strongly chalcophile elements will be affected depends upon the sulfur saturation status of the silicate melt, which is, in turn, a function of pressure, temperature and FeO abundances in the silicate melt (e.g. Wendlandt, 1982; Mavrogenes and O'Neill, 1999; O'Neill and Mavrogenes, 2002). The metasomatism-induced alterations of HSE and chalcophile element systematics may not be ubiquitously associated with lithophile element metasomatic

157 signatures, where bulk-rock geochemistry and textural features may disguise a refertilized
158 harzburgite as a fertile or modestly melt-depleted lherzolite.

159 Compared to studies of HSE, high precision analyses of Se and Te in peridotites are
160 scant and are dominated by Se abundance measurements (Morgan, 1986; Lorand et al.,
161 2003a, 2004; Lorand and Alard, 2010; Alard et al., 2011; Delpech et al., 2012; König et al.,
162 2012, 2014; Wang et al., 2013; Wang and Becker, 2013; Marchesi et al., 2013). The majority
163 of these studies have focussed on peridotite that include samples displaying unequivocal
164 evidence of metasomatism and / or refertilization by silicate melts. This potentially makes it
165 difficult to reconcile PUM concentrations of Se and Te with those drawn from
166 cosmochemical observations of chondritic meteorites (Lodders et al., 2009), when the
167 influence of metasomatism in terrestrial peridotites is considered.

168 This study focuses on a suite of well characterized peridotite xenoliths from
169 Kilbourne Hole, New Mexico, USA – the first comprehensive study of HSE, S, Se and Te in
170 basalt-hosted peridotite xenoliths. Prior investigations into their Re-Os isotope signatures
171 (Harvey et al., 2011) and lithophile element and Sr-Nd isotopic characteristics (Harvey et al.,
172 2012) have revealed that the composition of approximately half of the suite of xenoliths
173 retain geochemical characteristics consistent with melt depletion, but have subsequently
174 experienced small amounts of cryptic silicate metasomatism. The remainder have
175 experienced varying but, in general, greater degrees of cryptic silicate metasomatism, i.e.,
176 sufficient interaction with a melt to raise the abundances of the most incompatible lithophile
177 trace elements, but not intense enough to trigger the replacement of existing phases, or the
178 precipitation of new ones. These two sub-sets of Kilbourne Hole peridotites are evaluated for
179 their utility in estimating the HSE and chalcophile element characteristics of PUM, and the
180 degree to which metasomatic processes that affect the lithophile elements also disturb HSE
181 and chalcophile element signatures in melt depleted peridotites.

2. Geological setting and sample description

2.1 Geological setting

One of several late Pleistocene volcanic maars, Kilbourne Hole is situated in the Potrillo volcanic field on the axis of the Rio Grande Rift, which extends for more than 1000 km through south-western USA and onwards into northern Mexico. The lava flows at Kilbourne Hole (dated at 80 ± 10 kyr to 141 ± 75 kyr; Hoffer, 1976; Dromgoole and Pasteris, 1987; Bussod and Williams, 1991; Thompson et al., 2005) contain abundant peridotite and pyroxenite xenoliths. The lithosphere in this region is particularly thin, with estimates ranging from 40 km (Cordell et al., 1991) to 50-70 km (Keller et al., 1990). On the basis of gravity and teleseismic investigations (Keller et al., 1990; Olsen and Morgan, 1995), the crust at Kilbourne Hole is ca. 26 km thick, constraining the thickness of the underlying sub-continental lithospheric mantle (SCLM) to between 14 and 44 km. Geothermometry calculations based upon Ca exchange between orthopyroxene and clinopyroxene (Wells, 1977; Brey and Kohler, 1990) suggest that Kilbourne Hole xenoliths last equilibrated at temperatures ranging from 880 to 1180°C (Bussod, 1981; Kil and Wendlandt, 2004; Anthony et al., 2002; Harvey et al. 2012). When projected onto a calculated present-day geotherm (Decker and Smithson, 1975; Reiter et al., 1986) these temperatures suggest that equilibration last occurred at depths in excess of 48 km (Kil and Wendlandt, 2004). This is consistent with minimum entrapment pressures of 1.3 GPa obtained from olivine-hosted fluid and melt inclusions (Schiano and Clocchiatti, 1994). The asthenosphere-like Re-Os isotope signature of Kilbourne Hole xenoliths (cf. Harvey et al., 2006 and Harvey et al., 2011) also suggests that they were derived from close to the local lithosphere-asthenosphere boundary.

207

208 2.2. Bulk rock sample description

209

210 The samples examined in this study (n = 17) are a subset of Cr-diopside spinel-
211 lherzolites and spinel-harzburgites with predominantly protogranular textures from Harvey et
212 al. (2011, 2012), where detailed descriptions can be found (for lithology, texture, mineralogy,
213 modal abundances and equilibration temperatures see Table S1). The samples were selected
214 to represent as wide a range of clinopyroxene modal abundance (a field proxy for melt
215 depletion) as possible. No discrete metasomatic phases (e.g. phlogopite, amphibole, apatite)
216 were detected during this, or any prior study of this locality. Most samples have silicate
217 modal abundances consistent with varying degrees of melt depletion. However, two samples
218 (KH03-3 and KH96-8) plot significantly away from this trend (Figure 1), while a further four
219 peridotites (KH03-11, KH03-16, KH96-18 and KH96-24) are not consistent with derivation
220 from one melting event, but more likely multiple episodes of low degree (≤ 4%) partial
221 melting (Harvey et al., 2012).

222 Highly silicic, CO_2-S-saturated, alkali-enriched melts, found as inclusions, interstitial
223 glass or small veins have been observed in previous studies of some Kilbourne Hole
224 peridotite xenoliths (Schiano and Clocchiatti, 1994) e.g. KH03-15 (see Figure 4 in Harvey et
225 al., 2012). Olivine grains in contact with the veins appear to have been partially resorbed in
226 places, suggesting a degree of compositional disequilibrium between the primary mineral
227 assemblage and the secondary glass. KH03-10, KH03-15, KH03-21, KH03-24 and KH03-27
228 have all been observed to possess spongy clinopyroxene grain boundaries in close proximity
229 to the basaltic rind on the outside of the xenoliths, whereas in KH03-15, KH03-16 and KH03-
230 21 discrete stringers, veinlets and pockets of interstitial glass have been observed (Harvey et
231 al., 2012). Ten of the samples in this study have bulk-rock $(La/Yb)_N$, i.e., La/Yb normalized

232 to values of Primitive Mantle (McDonough and Sun, 1995) of <1 (Table S2; Figure 2a). This
233 subset of samples will be referred to as group 1 peridotites throughout the manuscript. The
234 remainder (n=7) have $(La/Yb)_N$ ranging from 1 to 4.7 (Table S2). This subset will
235 subsequently be referred to as group 2 peridotites. Interestingly, the La/Yb ratios are negatively
236 correlated with the whole-rock Al_2O_3 contents in both groups, implying that harzburgites are
237 systematically characterised by higher $(La/Yb)_N$ than the lherzolites in both group 1 and group 2
238 Kilbourne Hole peridotites. The osmium isotope ratios of both of the subsets of peridotites co-
239 vary strongly with indices of melt depletion (Harvey et al., 2011; Table S2; Figure 2b),
240 although group 2 samples project to $^{187}Os/^{188}Os$ in excess of that of PUM (Becker et al.,
241 2006). In addition, group 2 peridotites have much more scattered Re/Os ratios for a given
242 degree of melt depletion (Table S2; Figure 2c). This contrasts with group 1 peridotites whose
243 Re/Os co-variation with melt depletion is almost as strong as that between the Os isotope
244 ratios and bulk-rock Al_2O_3.
245
246 2.3 Sulfide petrology
247
248 The petrology of Kilbourne Hole BMS is described in detail in Dromgoole and
249 Pasteris (1987). Major element compositions (Table S3) and Re-Os isotope and elemental
250 systematics (Table S4) of BMS recovered from the Kilbourne Hole peridotite xenoliths used
251 in this study are described in detail in Harvey et al. (2011). Their petrological and
252 geochemical characteristics are summarized briefly here. Based upon major element
253 chemistry, BMS mineralogical assemblages can be divided into the following groups (see
254 Figure 4 of Harvey et al., 2011); Ni-rich and Ni-poor monosulfide solid solution (MSS) with
255 low (0.08–4.68 wt. %) Cu abundances, broadly equivalent to similar BMS elsewhere (Luguet
256 et al., 2003, 2004), and Cu-rich sulfides, analogous to chalcopyrite / cubanite from previous

studies of both mantle xenoliths and tectonically-emplaced peridotites (Dromgoole and Pasteris, 1987; Luguet et al., 2003, 2004). This second subset have very high Fe:Ni ratios and plot significantly below the array of the MSS grains. A single BMS grain with a composition similar to that of the basalt hosted sulfide of Burton et al. (1999) is also illustrated in Figure 4 of Harvey et al. (2011). However, this BMS was observed 1 cm inside a xenolith (KH03-23) and not in the host basalt. This demonstrates that in several xenoliths there has been limited ingress of the host basalt, but in all cases this is a minor effect. In addition to peripheral physical ingress of basaltic melt, a volatile-rich Te-bearing reaction may penetrate further into the xenoliths, capable of precipitating Te-bearing platinum group minerals (PGM; König et al., 2014).

Most of the BMS observed in the course of this study and Harvey et al. (2011) have, to some extent, experienced supergene weathering (Figure 3) where the sulfide minerals have been replaced by amorphous Fe-oxyhydroxide, i.e., [$FeO(OH)_5$-$6H_2O$], analogous to that reported by Luguet and Lorand (1998), Lorand et al., (2003a) and Alard et al. (2011). The BMS featured in Figure 3 is in fact one of the least weathered interstitial BMS grain observed during the course of this study. The exception to this is occasional small (< 50 µm) rounded to ovoid-shaped sulfides which appear to be wholly enclosed within a silicate grain, typically high Mg# (0.92) olivine, and thus protected from the effects of supergene weathering. These grains can be considered as representing < 5% of sulfides (cf. Alard et al., 2002; Alard et al. 2011), the remaining 95% being interstitial pentlandite and Cu-Ni -rich BMS.

Sulfides from 4 of the group 2 xenoliths (KH03-15, KH03-16, KH03-21 and KH03-24) were analysed for Re-Os isotope and elemental systematics in Harvey et al. (2011). Their Os concentration (i.e., [Os]) varies from 0.001 to 36.85 µg g^{-1} (Table S4). Rhenium concentrations range from 0.002 to 138.9 µg g^{-1} (Table S4). Osmium isotope ratios of the BMS grains range from 0.1185 to 0.3729, with wide ranges of values within individual

xenoliths (Table S4). Rounded, subrounded or euhedral sulfides, i.e., those most likely to have been enclosed within a silicate grain, have unradiogenic $^{187}Os/^{188}Os$ values, slightly below or indistinguishable from the bulk-rock Os isotope ratio, and usually have the highest [Os] and low [Re]. The remaining BMS have at least one straight edge, consistent with an interstitial nature, and are characterised by radiogenic Os isotope ratios, i.e., in excess of the corresponding bulk-rock value. They have up to two orders of magnitude lower [Os] and higher [Re] than the rounded sulfides (Harvey et al., 2011).

3. Analytical methods

3.1. Highly Siderophile Element abundance determination.

Bulk-rock HSE analyses were carried out at the Steinmann Institute für Geologie, Mineralogie und Paläontologie, Rheinische Friedrich-Wilhelms Universität Bonn on a 1 g powder split from the same material prepared for the previous studies of Harvey et al. (2011, 2012), where selected Ru and Os abundances, and $^{187}Os/^{188}Os$ had already been obtained, using methods described therein. A mixed ^{190}Os–^{185}Re–^{191}Ir–^{99}Ru–^{194}Pt–^{106}Pd-enriched spike was added prior to digestion. Digestions were performed in reverse aqua regia (5 mL 16 N HNO_3 and 2.5 mL 12 N HCl) for 14 h at 270 °C using an Anton Paar high pressure asher. After HP-asher digestion, the aqua regia fraction was further digested overnight using HF/HNO_3 in order to improve the digestion of the silicate minerals and maximise the recovery of Re. The HSE in this aqua regia fraction were subsequently separated and recovered by anion-exchange column chemistry (AG1X-8 100–200 mesh) using the methods described in detail in Dale et al. (2008, 2012, and references therein). This chemical separation is based on the procedure described by Pearson and Woodland (2000) and was

307 further modified by adding HF/HCl elution steps to improve the HFSE/HSE separation
308 (König et al., 2012; Lissner et al., 2014). Platinum, Ir, Re, Ru and Pd were analysed at the
309 Steinmann Institute on a Thermo Scientific Element XR SF-ICP-MS. Accuracy and precision
310 were tested by replicate analyses of UB-N peridotite (Meisel et al., 2003; Meisel and Moser,
311 2004). Precision is ±1% for Ir, ca. ±5 % for Pt and Pd and ca. ±15% for Re for the UB-N
312 triplicate analyses. Similar "low" Re reproducibilities were observed by Fischer-Gödde et al.
313 (2010) and attributed to powder heterogeneity inherent in the UB-N reference material. Total
314 analytical blanks (n=3; Table 1) were measured by isotope dilution for each set of chemistry.
315 The average blank values are 0.002 ± 0.001 ng for Ir, 0.022 ± 0.004 ng for Pd, 0.01 ± 0.005
316 and 0.006 ± 0.001 ng for Re. For the HSE, blank measurements represent less than 1 % of the
317 analysed unknowns and therefore a blank correction has not been applied. For peridotites
318 with the lowest Re abundances the blank can constitute up to 30% of the measured value
319 (KH03-25 and KH03-15), and in the exceptional case of KH03-16, with a measured Re
320 abundance of 0.007 ng g^{-1} the sample is barely distinguishable from the blank. As such, Re
321 abundances have been blank corrected (Table 2).
322
323 3.2. S-Se-Te abundance determination.
324
325 Sulfur abundance was determined using a LECO SC230 analyzer at University of
326 Leicester. Approximately 2 g of powder was made into a pellet and analysed in a He
327 atmosphere. Internal reproducibility was typically ± 0.5 to 0.8 µg g^{-1}. For the highest S
328 abundances (130 µg g^{-1}) this represents a maximum of ± 0.3 %. For KH03-16, the peridotite
329 with the lowest sulfur abundance ([S] = 3 µg g^{-1}) this internal reproducibility constitutes a
330 maximum of ± 26 %. For Se and Te abundance measurements, made at Rheinische Friedrich-
331 Wilhelms Universität Bonn, the peridotites were spiked with ^{77}Se and ^{125}Te isotope tracers

and digested according to the methods described in detail in König et al. (2012, 2014). Briefly, 1 g of sample powder was desilicified, using HF and concentrated HNO_3 in a bench top digestion procedure after complete digestion in inverse aqua regia using an Anton Paar high pressure asher at 100 bar and 220 °C for 12 h. Selenium and tellurium were separated using thiol cotton fibre (Yu et al., 1983) according to the method described in detail by König et al. (2012, 2014), using separation procedures modified from Marin et al. (2001), Elwaer and Hintelmann (2008), and Savard et al. (2009). Generally, the recovery of Se varied between 60% and 90%, while Te recovery varied between 10% and 90%. ^{77}Se, ^{78}Se, ^{125}Te and ^{126}Te were measured using a Thermo Scientific SF-ICP-MS Element XR equipped with a modified hydride generator (see Wombacher et al., 2009 and König et al., 2012 for details). Instrument parameters are documented in detail in König et al. (2012, 2014). The reproducibility of UB-N, [Se] of 132 ± 11 ng g^{-1} is indistinguishable from previous literature values (Terashima and Imai, 2000; Marin et al., 2001; Savard et al., 2009; Lorand and Alard, 2010; König et al., 2012, 2015a; Wang et al., 2013; Lissner et al., 2014). The Te concentration of UB-N is 10.20 ± 3.79 ng g^{-1}, again well within the previous reported range of values (Terashima, 2001; Lorand and Alard 2010; König et al., 2012). The Se/Te ratio therefore ranges between 8.6 and 22.3, again in complete agreement with previously published values (König et al., 2012; Wang et al., 2013). Total analytical blanks were indistinguishable from background intensities during analysis. This is broadly equivalent to ca. 0.1 ng g^{-1} for Se and 0.01 ng g^{-1} for Te, as based on background-corrected signal intensities for standard solutions of these concentrations (König et al., 2015a) and, as such, no blank corrections were made to the abundance measurements of Se and Te. Instrumental mass bias was corrected using natural $^{77}Se/^{78}Se$ of 0.3211762 and natural $^{125}Te/^{126}Te$ of 0.376728 (De Bièvre and Taylor, 1993).

4. Results

Sulfur, selenium and tellurium abundance for the 17 peridotite xenoliths are presented in Table 2. In summary, S concentrations range from 3 µg g^{-1} in KH03-16 to 130 µg g^{-1} in KH03-18, i.e., all samples in this study have S abundances significantly below estimates for the Primitive Mantle (PM = 250 ± 50 µg g^{-1}; Lorand, 1990; O'Neill, 1991; Palme and O'Neill 2003). There is no obvious relationship between S and Al_2O_3 (Figure 4). While most of the peridotites define a broad positive co-variation between S and Al_2O_3, there are samples in both subsets which extend to higher S abundances for a given Al_2O_3. Selenium abundances vary from 1.1 ng g^{-1} in KH03-16 to 56.9 ng g^{-1} in KH03-10. Duplicate measurements of Se abundances in group 1 peridotites do not reproduce as well as those of group 2 peridotites (Table 2) or the long term reproducibility of the UB-N reference material (cf. Table 1 and König et al., 2012, 2014, 2015a). A strong positive correlation is evident between the Se and S abundances in both the subsets of peridotites, i.e., R^2 = 0.88 and 0.92 for group 1 peridotites and group 2 peridotites, respectively (Figure 5). While stronger than the co-variation between S and Al_2O_3, the correlation coefficients between Se and Al_2O_3 are only marginally greater for both subsets of samples, with two samples from each subset (KH03-10, KH03-18, KH96-8, KH96-24) having particularly high Se concentrations for a given Al_2O_3 abundance (Figure 4b). Tellurium abundances range from 0.2 ng g^{-1} in KH03-16 to 19.2 ng g^{-1} in KH03-7. With the exception of KH03-7, there is a much more precise reproducibility of Te abundances in group 1 peridotites than there is Se. Group 2 peridotites, on the other hand, have compable and excellent Se and Te reproducibility (Table 2). Consequently, Se/Te ratios are much much scattered in group 1 peridotites than group 2 (Figure 5). There is a strong positive co-variation between Te and S abundances in group 2 peridotites (R^2 = 0.78) but no such relationship is apparent in group 1 peridotites (R^2 = 0.08;

382 Figure 5b). There is remarkably little covariation between Se and Te abundances in group 1
383 peridotites (R^2 = 0.11; Figure 5c) but there is a relationship in the group 2 peridotites, where
384 the R^2 is 0.60 (Figure 5c). Like S and Se, there is no strong co-variation between Te and
385 Al_2O_3 abundance (Figure 4c). Overall, the Kilbourne Hole peridotites from both group 1 and
386 group 2 define a similar Se/Te vs. Te trend as the one defined by König et al., (2012; 2014),
387 which include lherzolitic and harzburgitic peridotites from both xenolith localities (cratonic
388 and non-cratonic), and tectonically-emplaced massifs.

389 Highly siderophile element abundances can be found in Table 2 and are illustrated in
390 Figure 6. In general, HSE abundances are somewhat lower than current estimates for the
391 Primitive Upper Mantle (Becker et al., 2006). Interestingly, these HSE concentration
392 intervals and the PUM-normalized HSE patterns differ between group 1 and group 2
393 peridotites. The group 1 peridotites show sub-parallel HSE patterns with a surprisingly large
394 range of Ir contents (ca. one order of magnitude) along with more typical but still large
395 variations in Pt, Pd and Re concentration. All the group 1 peridotites show sub-PUM Pt/Pd
396 ratios (Becker et al., 2006), becoming more fractionated with decreasing Pt and Pd
397 concentrations. In comparison, the group 2 peridotites are characterised by Ir concentrations
398 varying by up to 40% and are variably depleted in Pt, Pd and Re. Independently of their
399 $(La/Yb)_N$ ratios, all the Kilbourne Hole peridotites are characterised by sub-PUM $(Os/Ir)_N$
400 (i.e., 0.42-0.84). Excluding KH03-24, these $(Os/Ir)_N$ correlate inversely with Pd depletion and
401 the $(Pd/Ir)_N$ ratios for the group 2 peridotites. $(Ru/Ir)_N$ ratios are also significantly lower than
402 PUM ranging from 0.93 in KH03-21 to 0.78 in KH03-16. Furthermore, strong correlations
403 are evident for group 1 peridotites between Os and Ir (Figure 7a), Pt and Pd; (Figure 8b), Re
404 and Pt or Pd (Pt; Figure 7c) and between Ir and Pt (Figure 7d). The peridotites from group 2
405 also display a positive correlation between Pd and Re; and Pd and Ir (excluding KH03-24).
406 However, unlike group 1 peridotites, group 2 peridotites exhibit negative correlations

between Ir and Os vs. Pd. Most of the group 2 peridotites are indistinguishable from the group 1 peridotites with respect to Os vs. Ir abundances; only the most depleted group 1 peridotites are shifted toward higher Os concentrations for a given Ir contents. Only 3 samples, all group 2 peridotites, have $(PPGE/IPGE)_N$ >1; KH03-3 and KH96-8 both have $(Pt/Ir)_N$ >1, whereas KH03-3, KH96-8 and KH03-24 have $(Pd/Ir)_N$ >1 (where PPGE = Pd and Pt, and IPGE = Os and Ir; Barnes et al., 1985).

A strong positive correlation between S and Pd abundances is evident (Figure 8a) in both subsets of peridotites (R^2 = 0.78 for group 1 peridotites; R^2 = 0.80 for group 2 peridotites). A similar, although less strong relationship in group 2 peridotites, is also observed between Pd and Se (Figure 8b). However, the converse is seen in the relationship between Pd and Te - there is a much stronger correlation between these two elements in group 2 peridotites (R^2 = 0.92) than in group 1 peridotites (R^2 = 0.28; Figure 8c). The relationships between Re and S, and Se and Te are also striking (Figure 8d, e and f, respectively), although there is no correlation between Re and Se in group 2 peridotites; Figure 8e). Neither of the subsets of peridotites show any strong correlations between $(La/Yb)_N$ and S, Se, Te or PPGE, although group 2 peridotites are more strongly (negatively) correlated with $(La/Yb)_N$ than group 1 peridotites (Figure 9). The only elements that deviate from this pattern are the IPGE, which have slight (R^2 = 0.13) to moderate (R^2 = 0.53) positive co-variations with $(La/Yb)_N$. However, no such co-variation between IPGE abundance and S, Se or Te concentration is apparent

5. Discussion

5.1 The effects of hydration, volatilization, and supergene weathering

Peridotite xenoliths are randomly sampled by basaltic melts that ascend through the lithosphere. They are often extremely fresh, especially so in the case of Kilbourne Hole peridotites. No serpentinization or discernable alteration of the silicates or spinel was observed. In fact all of the samples exhibited modest gains on ignition (see online supplementary information in Harvey et al., 2012). While the possibility exists for interaction with, or infiltration of the host basalt (for which some evidence is preserved in the rims of KH03-10 and KH03-27; Table S5), and it has been suggested that high temperatures associated with entrainment in the host basalt may trigger devolatilisation, or partial loss of S and perhaps Se (e.g. Lorand et al., 2003a, Alard et al., 2011), sampling from the centre of these >1 kg xenoliths (Harvey et al., 2011, 2012) avoids these potential complications, which tend to be restricted to the outermost centimetre or so of the xenoliths.

Sulfur abundances are, in general, lower than the array of mostly orogenic peridotites from the literature (Le Roux et al., 2007; Lorand et al., 2010; Alard et al., 2011; König et al., 2012, 2014; Wang et al., 2013) but overlap with the previous Kilbourne Hole study of Morgan (1986), despite the latter study having higher S concentrations for a given level of Al_2O_3. Unlike orogenic peridotites, none of the Kilbourne Hole peridotites have S abundances in excess of the estimated Primitive Mantle value of (250 ± 50 µg g^{-1}). This shift to lower S abundances than orogenic peridotites is likely due to supergene weathering (Figure 3). This phenomenon was also observed in xenoliths from the French Massif Central by Lorand et al (2003a), who used Se abundances as a proxy for mantle S abundance in similar xenoliths. The poor correlation with silicate dominated indices of melt depletion, such as Al_2O_3, is not helped by the clear perturbations to sulfide modal abundances in these peridotites which have been modified since melt depletion by the addition of metasomatic sulfide, and the subsequent removal of sulfide in a S-undersaturated melt (see section 5.2, below).

457 At the bulk-rock scale, Os and Ir are not fractionated by magmatic processes as both
458 are hosted by BMS (i.e MSS, pentlandite). However, the IPGE may behave differently at the
459 microscale when alloys have been stabilised in response to the disappearance of BMS during
460 a high degree of partial melting. In the Kilbourne Hole xenoliths melt depletion does not
461 extend to the high degrees (> 25%) often required for the formation of refractory alloys.
462 However, while the degassing of highly volatile OsO_4 during the eruption of the host basalt
463 could be implicated in the loss of Os from these xenoliths (e.g. Lorand et al., 2003b), this
464 process requires highly oxidizing conditions (fO_2 > hematite-magnetite buffer) only found in
465 arc volcanics (e.g. Frost and McCammon, 2008).
466 Supergene weathering of BMS is, therefore, the most likely cause of the low Os
467 abundances and sub-chondritic Os/Ir ratios observed at Kilbourne Hole (cf. Handler and
468 Bennett, 1999; Pearson et al., 2004). Moreover, as has been inferred in several prior studies
469 of siderophile and chalcophile elements in peridotite xenoliths (e.g. Lorand, 1990; Lorand et
470 al., 2003a, 2003b; Reisberg et al., 2005; Alard et al., 2011), sub-chondritic S/Se ratios are a
471 function of the increased affinity of S for O over that of Se for O (Dreibus et al., 1995;
472 Lorand et al., 2003a). This in turn means that groundwater or meteoric water percolating
473 through peridotite xenoliths has the potential to remove sulfide as sulfate whilst leaving Se
474 abundances less affected. For BMS apparently enclosed within olivine or orthpyroxene, the
475 silicate "armor" should provide a degree of protection against supergene weathering but, just
476 like silicate melt and fluid inclusions (e.g. Bodnar, 2003), BMS inclusions hosted within
477 peridotite xenoliths may experience decrepitation induced by the rapid drop in pressure
478 associated with the entrainment of a xenolith and its transport to the surface (e.g. Andersen et
479 al., 1987). Griffin et al. (2002) noted that many BMS grains in peridotite xenoliths from the
480 Siberian craton, especially the larger sulfides, show radiating expansion cracks lined with
481 films of sulfide, which may provide a pathway for meteoric water to interact with seemingly

enclosed BMS grains. This permits the partial oxidation sulfur to sulfate and Os to OsO_4 and the removal of both species. This low temperature alteration process does not seem to have any measurable effect on the lithophile trace element systematics, the majority of the HSE, or the silicate (± spinel) mineralogy. In other words, only Os and S are clearly disturbed, to any measurable degree, by supergene weathering.

However, Se may not be completely immobile under these conditions, but still less mobile than S (Alard et al., 2011). For example, Figure 3 shows that BMS oxidation has taken place, but Figure 5a demonstrates that many of the Kilbourne Hole samples retain a chondritic, or near-chondritic S/Se ratio, but with low bulk-rock S abundances. For example, in a recent study of peridotite xenoliths from Montferrier, Southern France (Alard et al., 2011), several xenoliths yielded very low Se contents for a given sulfur abundance. This suggests that peridotite xenoliths may also lose Se during the transport of xenoliths in their host basalt or as a result of supergene weathering (cf. Lorand et al., 2003a). König et al. (2014) discussed the possibility that near chondritic Se/Te ratios in fertile peridotites are not a primitive signature of the Earth's mantle, but rather reflect strong enrichment in metasomatic phases which accommodate high abundances of chalcogens, which erased previous pristine melt depletion signatures. This is supported by near-chondritic Se/Te signatures in metasomatic Cu-Ni-rich sulfides compared to much high Se/Te in residual sulfides (Se/Te ≤ 200). Moreover, interstitial PGM-bearing fine fractions of a depleted peridotite also show exclusively low Se/Te compared to residual Se-Te host phases in olivine (König et al., 2015a). There is some support for this hypothesis in the Se/Te systematics observed in the group 1 peridotites at Kilbourne Hole. However, in the group 1 peridotites, where an additional process lowered the Se/Te, a low Se/Te ratio could be generated in at least two different ways, i.e., by loss of Se (Alard et al., 2011) where the Se/Te was lowered from a

506 supra-chondritic ratio to near chondritic (ca. 9) or, conversely, with the addition of Te, which
507 is discussed in the sections that follow.
508
509 5.2 High temperature processes affecting peridotite compositions
510
511 5.2.1 Rare Earth Element signatures of melt depletion and subsequent metasomatism
512
513 The peridotites in this study have been divided into two sub-groups, based upon their
514 $(La/Yb)_N$, i.e., the La/Yb ratio normalized to Primitive Mantle (McDonough and Sun, 1995).
515 Group 1 peridotites are identified by a $(La/Yb)_N$ of <1, whereas group 2 peridotites have
516 $(La/Yb)_N$ of >1. The simplest interpretation of a peridotite with a $(La/Yb)_N$ of <1 would be
517 that it retains the signature of melt depletion without overwhelming subsequent metasomatic
518 disturbance. A small amount of cryptic metasomatism is possible, but there are limits to its
519 extent; high degrees of silicate metsomatism could raise $(La/Yb)_N$ to values in excess of 1,
520 but this is dependent upon the nature of the metasomatic agent. Alternatively, the influx of a
521 LREE-depleted basalt, such as a MORB or similar, at high-melt-rock ratios may also mimic
522 the effects of varying degrees of melt depletion in peridotites (e.g. Seyler et al. 2001, 2007;
523 Bodinier and Godard, 2003). Such high melt/rock ratios can be obscured by subsequent
524 recrystallization (e.g. Soustelle et al., 2009). However, despite the rift-like setting of
525 Kilbourne Hole, there is no clear evidence (e.g. low bulk-rock or mineral Mg#), to suggest
526 this is the cause of the observed REE element systematics in the group 1 peridotites.
527 However, alone, $(La/Yb)_N$ can be insensitive to the effects of small amounts of
528 metasomatism. Despite a lack of supporting petrographic evidence for metasomatism in the
529 group 1 peridotites (see Harvey et al., 2012 and Table S5, this study), the absolute
530 abundances of La, Yb and Al_2O_3 in group 1 peridotites, without exception, possess higher

531 $(La/Yb)_N$ for a given Al_2O_3 abundance to have been produced by melt depletion (Figure 2a).
532 Hence, a melt-depletion signature, albeit slightly modified by cryptic metasomatism, is the
533 most likely cause of the observed REE signature.

534 This feature is even more pronounced in the group 2 peridotites but, in some cases, is
535 also accompanied by several lines of petrographic evidence for metasomatic processes
536 subsequent to melt depletion (Table S5; Harvey et al., 2012). It should be noted though that
537 using the La/Yb ratios as proxy of "metasomatism" probably exaggerates the degree of
538 metasomatic overprinting in the group 2 harzburgites; their HREE are much lower than any
539 other peridotites from the Kilbourne Hole suite (Harvey et al., 2012). It is possible that the
540 group 2 harzburgites are the only peridotites to have preserved some "intact" HREE
541 abundances. Their low HREE abundances point to ≤25 % partial melting at low pressure (1-3
542 GPa), and the slight "spoon" shape argues for addition of only the most incompatible REE
543 (see Figure 9 in Harvey et al., 2012). In terms of the REE, the group 2 harzburgites may form
544 a continuum starting with metasomatism by small fractions of incompatible element-rich melt
545 fractions in the group 2 harzburgites, leading to larger melt fractions being added to the group
546 2 lherzolites.
547
548 5.2.2 Chromatographic fractionation of REE during melt/rock interaction
549
550 The interpretation of elevated $(La/Yb)_N$ resulting from simple mixing of residual
551 peridotite with a silicate melt is likely to be overly simplistic in some cases. A consequence
552 of the low incompatible trace element abundances in residual peridotite is that the xenoliths
553 that record the greatest degree of melt extraction (those with the lowest Al_2O_3 and / or Yb)
554 are the most susceptible to having their melt depletion signature overprinted by subsequent
555 incompatible element metasomatism (Wood and Blundy, 2003) as a result of their inability to

556 buffer against an influx of highly incompatible elements present in, for example, a C-O-S-H-
557 enriched silicate melt (Alard et al., 2011). Figure 2a demonstrates that the most depleted
558 peridotites have the highest $(La/Yb)_N$ in both sample subsets, i.e., despite a major element
559 signature reminiscent of melt depletion, they have acquired an enrichment of LREE over
560 HREE. Navon and Stolper (1987) and Bodinier et al. (2004) have both quantified a
561 chromatographic effect observed in melt-depleted peridotites where LREE/HREE are
562 predicted to increase away from the site of intense melt-peridotite interaction, such as during
563 the generation of pyroxenite found at Kilbourne Hole, both as discrete and composite
564 xenoliths (Dromgoole and Pasteris, 1987; Wilshire et al., 1988; Kil and Wendlandt, 2004).
565 Since fronts of the more incompatible elements travel faster through the adjacent peridotite,
566 their concentrations rise earlier. A clear distinction between addition of small amounts of a
567 silicate melt back into a depleted peridotite pre-cursor versus cryptic modification of
568 incompatible trace element abundances is difficult to resolve. However, in the peridotites
569 with the lowest Al_2O_3 abundance and highest $(La/Yb)_N$, a chromatographic effect from a
570 proximal melt-peridotite interaction seems more feasible.

571 The two trends illustrated by groups 1 and 2 in Figure 2a project back to a common
572 composition at ca. 5 wt. % Al_2O_3 and a very low $(La/Yb)_N$ that is inconsistent with a
573 Primitive Mantle composition. Using the lithophile elements alone, it is probably not possible
574 to unequivocally unravel the petrogenetic history of these peridotites, other than group 1
575 peridotites have experienced a smaller degree and less generations of silicate metasomatism
576 than group 2 peridotites. That the group 2 peridotites have experienced a more complex
577 petrogenetic history is supported by the extended REE and lithophile incompatible trace
578 element plots abundances (Harvey et al., 2012).

579

580 5.3 Processes affecting the highly siderophile element compositions of peridotites

While a general consensus exists regarding the nature of melt depletion and subsequent metasomatism with respect to the behavior of major (e.g. Baker and Stolper, 1994; Baker et al., 1995; Hirschmann et al., 1998; Robinson et al., 1998) and trace elements with a lithophile affinity (e.g. Blundy and Wood, 1994, 2003; Wood and Blundy, 2001), the role played by BMS during these processes is less well constrained, despite extensive experimental investigations into its behavior (e.g. Fleet et al., 1991, 1996; Peach and Mathez, 1993; Peach et al., 1994; Brenan, 2002, 2008; Brenan et al., 2003, 2005; Bockrath et al., 2004; Righter et al., 2004; Ballhaus et al., 2006; Holzheid, 2010; Mungall and Brenan, 2014). Mantle BMS in melt depleted peridotite constitute less than 0.1 modal % (corresponding to 250 ± 50 µg g^{-1} S) of the upper mantle (O'Neill, 1989; Lorand, 1990; Palme and O'Neill, 2003), yet their high $D^{sulfide/silicate}$ ensures that these accessory phases dominate the mass balance of bulk-rock peridotite for the HSE (e.g. Fleet et al., 1991, 1996; Peach and Mathez, 1993; Peach et al., 1994; Guo et al., 1999), and may also exert a strong control on the distribution of Pb in the mantle (Burton et al., 2012; Warren and Shirey, 2012).

The behavior of sulfur during partial melting of peridotite is assumed to be related to the steady depletion of BMS following a batch/equilibrium melting process (e.g. Morgan, 1986; Handler and Bennett, 1999; Lorand et al., 1999; Luguet et al., 2003; Pearson et al., 2004; Fischer-Gödde et al., 2011), resulting in a residual peridotite that is mostly devoid of BMS and sulfur at around 25 % partial melting (e.g. Burnham et al., 1998). During partial melting, BMS melts incongruently to produce a refractory monosulfide solid solution (MSS) that retains Os, Ir and Ru in the mantle residue, and Cu–Ni-rich sulfide melt (Barnes et al., 1997; Alard et al., 2000; Luguet et al., 2003; Bockrath et al., 2004; Peregoedova et al., 2004; Wang and Becker, 2015a) which hosts Pt, Pd and Re and is extracted within the partial silicate melts, although the exact importance of this fractionation during partial melting is not

606 universally agreed upon (Wang et al., 2013; Mungall and Brenan, 2014; Wang and Becker,
607 2015b). Therefore, partial melting residues are generally characterised by PUM-like or even
608 slightly elevated Os and Ir contents, but substantial and progressive depletions in Pt, Pd and
609 Re (see Lorand et al., 1999; Pearson et al., 2004; Luguet et al., 2007).

610 Three samples from the group 2 xenoliths (KH96-24, KH03-15 and KH03-16) show
611 such HSE patterns, which are consistent with moderate to high degrees (15-20 %) of partial
612 melting of a fertile peridotite (Figure 6b; cf. Figure 3 from Harvey et al., 2011). Interestingly
613 they are the most depleted peridotites of group 2 with Al_2O_3 contents < 2.7 wt.%. Although
614 Os was likely lost during the late supergene weathering, thus lowering the original Os/Ir
615 ratios, these three samples still retain the highest Os concentrations and tend to have the
616 highest $(Os/Ir)_N$ ratios, suggesting that some magmatic systematics may still be preserved.
617 High Os concentrations combined with high Os/Ir ratios (generally greater than PUM) may
618 be symptomatic of the stabilisation of laurite (Ru-Os sulfide) and subsequent Os-Ru rich
619 alloys forming in response to the complete exhaustion of BMS in the mantle residue during
620 extensive partial melting (ca. c. 20-25%; Luguet et al., 2007). The exhaustion of sulfides in
621 these three samples is supported by the low to extremely low bulk-rock sulfur abundances of
622 these three peridotites ([S] in KH96-24, KH03-15 and KH03-16 = 3 to 36 µg g^{-1}, Table 2).

623 The remaining 4 peridotites of group 2 have HSE patterns, with either flat to elevated
624 Pd/Pt and/or Re/Pd, which are inconsistent with both their refractory nature (i.e., bulk rock
625 Al_2O_3 contents) and their sulfur abundances. These features, combined with the overall S vs.
626 HSE (especially Pd) and PPGE/Ir (i.e., Pd/Ir) correlations among these four samples may be
627 best explained by addition of metasomatic PPGE-rich BMS (similar to the interstitial Type-2
628 sulfides of Alard et al., 2002, 2011) to a predominantly melt-depleted residual peridotite.
629 Evidence for the addition of HSE to melt depleted peridotites (e.g., Becker et al., 2001;
630 Luguet et al., 2003, 2004; Pearson et al., 2004; Ionov et al., 2006; van Acken et al., 2008,

631 2010b), or their selective removal (Lorand et al., 2000; 2003a; 2004; Becker et al., 2001;
632 Büchl et al., 2002; Ackerman et al., 2009) is becoming increasingly abundant in the literature,
633 and this provides a framework within which the HSE abundances in Kilbourne Hole
634 xenoliths can be interpreted.

635 Assuming the addition of ca. 80 µg g^{-1} S (the whole-rock S contents of both KH03-3
636 and KH96-8) as metasomatic BMS in a S-free partial melting residue with a HSE
637 composition similar to the most depleted group 2 peridotite (KH03-16), the HSE systematics
638 of KH03-3 and KH96-8 can be reproduced if the metasomatic BMS hosts, on average, 20 µg
639 g^{-1} Pt and 25 µg g^{-1} Pd. These BMS contents are typical of Pt and Pd concentrations obtained
640 in BMS from peridotite xenoliths (Alard et al., 2000; 2002; Lorand and Alard, 2001; Alard et
641 al., 2011) or tectonically emplaced peridotite massifs (Luguet et al., 2001; 2004; Alard et al.,
642 2005). To account for the HSE systematics of KH03-24, the average metasomatic BMS must
643 be characterised by an even stronger Pd enrichment (45 µg g^{-1} Pd and 8 µg g^{-1} Pt). Such
644 compositions can also be found in xenolithic BMS (e.g. grains s15 and s13 from xenolith Mtf
645 37, from Montferrier, southern France; Alard et al., 2011).

646 Precipitation of BMS has been attributed to either percolation of S-saturated silicate
647 melts or to sulfidation reaction between a C-O-S-H fluids with magnesian silicates (e.g.
648 Ackerman et al., 2009; Alard et al., 2011; Delpech et al., 2012; Lorand et al., 2013). The
649 preservation of ≤ PUM S/Se and Pd/Pt ratios in the group 2 peridotites likely to have
650 experienced BMS precipitation strongly argue for percolation of a silicate melt and
651 precipitation of Cu-Ni-rich BMS rather than the volatile transport of S and HSE and
652 crystallisation of pyrrhotite-chalcopyrite assemblages (Delpech et al., 2012). Small-degree
653 melt fractions, preserved as melt inclusions, have previously been reported in Kilbourne Hole
654 xenoliths (Schiano and Clocchiatti, 1994). These are CO_2 saturated silicate melts (e.g.
655 Menzies and Dupuy, 1991; Moine et al., 2004), in addition to being S-saturated. In addition,

656 the group 2 peridotites have a slightly higher $^{187}Os/^{188}Os$ for a given Al_2O_3 abundance than
657 the group 1 peridotites (Figure 2b) which suggests that a Re-bearing phase, such as
658 metasomatic sulfide, may have been added sufficiently long ago to allow a small amount of
659 ^{187}Os ingrowth prior to removal of sulfide by a sulfur-undersaturated melt. Indeed, KH03-24
660 and KH96-8 both retain elevated Re-Os ratios (Figure 2c) compared to the rest of the two
661 groups of peridotite.

662 By contrast, the group 1 peridotites all preserve sub-parallel HSE patterns (Figure 6a)
663 and strong positive correlations between all of the HSE. This contrasts with the fractionated
664 HSE patterns (Figure 6b) and correlations between only IPGE or PPGE and Re in the group 2
665 peridotites (Figure 7). Although any individual group 1 peridotite may preserve a HSE
666 pattern that resembles a melt depletion signature, the parallel offset of the HSE patterns
667 within the group cannot be attributed to this process. Depending upon the degree of sulfur
668 saturation, a predominantly silicate metasomatic melt may dissolve sulfides located in
669 interstices between silicate minerals. The S-saturation concentration of lavas increases with
670 decreasing pressure, i.e., shallower depths (Mavrogenes and O'Neill, 1999), allowing S-
671 undersaturated silicate melt to pass through the SCLM. These S-undersaturated melts thus
672 have the potential to remove sulfide not enclosed inside silicates (e.g. Lorand and Alard,
673 2001; Lorand et al., 2003a, 2003b, 2004; Reisberg et al., 2004, 2005). This effect may be
674 enhanced by ongoing open-system melting associated with reactive porous flow at increasing
675 melt/rock ratios, which has the effect of diluting S in the percolating melt. The effect of
676 sulfide removal is likely to be a dilution of a pre-existing HSE signature, depending upon the
677 absolute amount of sulfide removal that has occurred. The parallel HSE patterns of the group
678 1 peridotites are consistent with this hypothesis. Following a period of melt depletion that
679 imparted a relatively uniform melt depletion signature upon the group 1 peridotites, a sulfur-
680 undersaturated melt passed through that portion of the SCLM, removing different proportions

681 of sulfide from the group 1 peridotites. This is not only consistent with the observation that
682 the peridotites with the lowest S abundances of the group (KH03-25, KH03-27, KH96-2,
683 KH96-18) have the lowest overall HSE content, but also that the group 1 peridotites have
684 well correlated IPGE versus PPGE abundances (Figure 7) and possess the lowest $(La/Yb)_N$,
685 implying that the precipitation of metasomatic phases or fingerprints was negligible in group
686 1 peridotites. This in turn is supported by the observation that there is little or no petrographic
687 evidence for the precipitation or crystallization of a metasomatic melt or fluid preserved in
688 the group 1 peridotites (Table S5); the removal of sulfide, and the HSE that it hosts, by a
689 transiting sulfur-undersaturated melt has simply diluted a pre-existing melt depletion
690 signature. It is not clear whether or not the group 1 peridotites experienced any addition of
691 PPGE-rich sulfide (cf. group 2 peridotites) prior to the passage of a sulfur-undersaturated
692 melt, but the parallel HSE patterns observed within this group of peridotites (Figure 6a)
693 suggests that this is unlikely.
694
695 5.4 The effects of melt depletion and subsequent processes on S-Se-Te systematics
696
697 Despite the potential to use S as a proxy for melt depletion (e.g. Burnham et al.,
698 1998), in instances where sulfide has been either added or removed, this usefulness quickly
699 becomes undermined. The only remaining evidence that S concentrations have not been
700 completely decoupled from silicate-dominated processes is found in those group 2 peridotites
701 which have experienced the greatest amount of melt depletion (KH03-15 and KH03-16). In
702 these examples, Al_2O_3, S and PPGE are all extremely low, despite a clear silicate-
703 metasomatic overprint (Figure 4a, Figure 9a, Figure 6, respectively). Similarly, there is very
704 little correlation between Se and Al_2O_3 (Figure 4b). The measured, broadly chondritic S/Se
705 ratios of this study are also consistent with previous measurements of Kilbourne Hole

peridotite xenoliths by Morgan (1986) (black circles, Figure 5a) and are within the range of published values of S/Se in the literature, which are dominated by orogenic peridotites, but which show a considerable degree of scatter at higher S and Se abundances, particularly where the concentrations of these elements exceed the estimates for a Primitive Mantle composition. Like sulfur, the Se systematics of both groups of peridotites have been decoupled from silicate indices of melt depletion, but the most highly melt depleted group 2 peridotites (KH03-15 and KH03-16) contain the lowest abundances of Se (Figure 4b). As Se is partitioned into interstitial pentlandite and chalcopyrite, the behavior of Se during melt depletion, sulfide addition and the removal of sulfide in a sulfur-undersaturated melt would be expected to mimic the behavior of the PPGE (e.g., van Acken et al., 2010a). This is demonstrated in Figure 8b where the strong co-variation of Se with Pd is illustrated for both groups of peridotites. The contrasting geochemical behavior of strongly compatible Ir ($D^{sulfide/silicate\ melt}$ ca. 5 x 10^4; Peach et al., 1994) and mildly compatible Se ($D^{sulfide/silicate\ melt}$ c. 10^3; Peach et al., 1990; Mungall and Brenan, 2014), cannot explain the distinct co-variation between these two elements in group 1 peridotites compared to invariant Ir abundance over a large range of Se abundance in group 2 peridotites. In the group 2 peridotites, enriched Se for a given Ir content may be the result of exsolution of a metasomatic Se-bearing Cu-Ni sulfide phase from a silicate melt containing virtually no IPGE, i.e., the addition of metasomatic sulfide after melt depletion. Precipitation of a metasomatic Cu-Ni-rich sulfide could also increase the Te abundances more dramatically than the Se in these samples, yet this is not observed; the Te abundances of group 1 and group 2 peridotites are indistinguishable, which in turn, suggests that Se and Te may be controlled by different phases in different groups of peridotites. This effect is compounded by the apparent vulnerability of Se to supergene weathering, compared to Te. These effects are best illustrated in Figure 5c, where large differences in the correlation coefficients between Se and Te for the two groups of peridotites

731 are observed. This, in turn, is consistent with the poorer reproducibility of Se and Te in
732 KH03-2 and KH03-7 (group 1 peridotites) where tellurides may control at least some of the
733 Te budget, compared with much more reproducible replicate analyses of group 2 peridotites
734 where Se and Te abundances are more strongly correlated (Figure 5c), the external
735 reproducibility of replicate analyses is stronger , and sulfide is the dominant host phase for Se
736 and Te (Figure 5a and b).

737 Although early studies suggested that the compatibility of chalcogenic elements varies
738 systematically, i.e., Te > Se > S (e.g., Hertogen et al., 1980; Morgan, 1986; Hattori et al.,
739 2002) subsequent investigations suggest the contrary, especially in harzburgites (König et al.,
740 2012, 2014). Tellurium does not appear to behave as coherently as S and Se with regard to
741 melt depletion and subsequent mantle processes, especially in the group 1 peridotites, most
742 likely because the distribution of Te is more strongly controlled by the heterogeneous
743 distribution of micron-sized tellurides than in group 2. Figure 4c shows that there is no
744 discernible co-variation of Te with Al_2O_3 over a wide range of melt depletion. In this respect,
745 the samples of this study overlap completely with those of Morgan (1986). Moreover, where
746 Al_2O_3 is greater than 1 wt. % the range of Te contents measured in Kilbourne Hole
747 peridotites overlap completely with the existing literature data derived from mostly orogenic
748 peridotites, and is otherwise unremarkable. Strong correlations between S and Te (Figure 5b),
749 and Se and Te (Figure 5c) are only observed in the group 2 peridotites. Both S/Te and Se/Te
750 plot on sub-chondritic trajectories, with the Se/Te of group 1 peridotites being particularly
751 low. This provides further evidence for the likely mobility of sulfide-hosted Se during
752 supergene weathering and interaction with a S-undersaturated melt, but is also testament to
753 the effects of telluride precipitation that are relatively unaffected by these processes. The
754 strong control exerted by metasomatic BMS on Te abundance (Helmy et al., 2010) is
755 illustrated by the positive correlations between Pd, Re and Te in group 2 peridotites (Figure

8). The sympathetic variation of S and PPGE in the group 1 peridotites clearly argue for the removal of all these elements during BMS dissolution in percolating S-undersaturated melts. The persistence of high Te concentrations in group 1 peridotites, and its decoupling from S and the PPGE, along with the poor reproducibility of the Te concentrations, demonstrates that Te is not significantly mobilized during the BMS dissolution because it is hosted in tellurides. Alternatively, Te may have been added after interaction with a sulfur-undersaturated melt. Late exhalative precipitation of tellurides from a volatile rich melt (cf. König et al., 2014) could also account for the observed Te systematics in the group 1 peridotites.

In residual sulfide-free harzburgites Se is entirely controlled by micro-inclusions of PGM in olivine (König et al., 2015a), but this host phase could equally be base metal sulfide trapped within silicate grains in less severely depleted xenoliths. Some Se from interstitial sulfides could be volatilized and lost, but the Se hosted in silicate-armored sulfide would be retained. Hence, bulk-rock Se abundance could still be low, yielding subchondritic Se/Te ratios. The only previously reported non-basalt-borne peridotites that also show subchondritic Se/Te (three harzburgitic samples from Lherz; König et al., 2012) have been strongly affected by the introduction of metasomatic Bi-Pt-telluride without Cu-Ni-rich sulfide precipitation, which may increase Te abundances but not necessarily Se to the same degree. In the group 1 peridotites, Se/Te remain relatively constant, but it is difficult to account for the very low Se/Te ratios in the group 1 peridotite that possess the highest Te abundance without the presence of tellurides (Figure 5).

Several authors have discussed the formation of PGM and their effect upon bulk-rock HSE (± Se-Te-As-Bi) abundances. A diagnostic feature of metasomatic processes is the increasing modal abundance of Pt–Pd–Te–Bi or Pt–As–S micro-phases, whereas refractory PGM, residual after intense melt depletion, may be represented by Ru–Os ± Ir sulfides and Pt–Ir ± Os alloys (Luguet et al., 2007; Kogiso et al., 2008; Wang et al., 2009; Ackerman et

al., 2009, 2013; Lorand et al., 2010, 2013; O'Driscoll et al., 2012). These phases are notoriously difficult to find using optical methods and even detailed studies of sulfide grains, or the spinel with which they are intimately associated, often fail to reveal their presence (e.g. Ferraris and Lorand, 2008). However, Wang et al. (2009) identified discrete Pt–rich micro-nuggets from in-situ analyses of enclosed MSS in xenoliths from the Penghu Islands (Taiwan). Ackerman et al. (2009) described the effects of Pt-rich discrete microphases in sulfide-poor melt-percolated Bohemian xenoliths, while Luguet et al. (2007) identified Cu-Rh-Pt sulfides in barely metasomatized orogenic harzburgites, and Lorand et al. (2010) described Ru‑Os ± Ir sulfides and Pt‑Ir ± Os alloys recovered from melt-percolated orogenic lherzolites and harzburgites from Lherz. Although no PGM consistent with BMS exhaustion have been detected in Kilbourne Hole xenoliths, the occasional presence in some xenoliths of low temperature PGM, such as Pd ± Pt-tellurides, is inferred from the anomalous PPGE-Te signatures observed in KH96-24 and KH03-24. KH96-24 has an unusually high Te abundance (14 ng g^{-1}; Table 2) but is otherwise unremarkable. Conversely, KH03-24 has a remarkably high Pd concentration (18 ng g^{-1}), which may be attributable to an alloy phase-derived nugget effect, but no corresponding elevated concentration of either Pt or Te is observed. Whether the occasional anomalous HSE signatures seen in the Kilbourne Hole xenoliths of this study can be attributed to PGM micro-nuggets or not or should only treated as speculation without firm identification of the PGM themselves. Lorand et al. (2010) suggest that every metsomatized peridotite also likely contains Pt-Ni-tellurides; while the Se-Te signatures of the group 1 peridotites support this hypothesis, further detailed work is necessary on this peridotites to unequivocally confirm this.

Figure 10 summarizes the likely sequence of events to have affected the HSE, Se and Te abundances in the Kilbourne Hole peridotites. Both groups of peridotite experienced ≤ 25 % melt depletion. In the case of group 1 peridotites, this was followed by interaction with a

S-undersaturated melt which removed BMS, thus leading to depletion in the observed PPGE and Se abundances. Tellurium was likely retained in micron-scale tellurides. Following melt depletion, group 2 peridotites interacted with an ascending C-O-S-H-rich melt or fluid, which added varying amounts of metasomatic PPGE (± Re ± Se ± Te)-bearing Cu-Ni-Fe sulfide; this results from the upward decrease in porosity and temperature in the SCLM with reduced depth, as described by Bedini et al. (1997). After exposure at the surface, both groups of xenoliths experienced loss of S and Os (± Se) as a result of supergene weathering. These features link the melt depletion signature preserved in the major element and HSE chemistry with the chromatographic effect of infiltration of a C-O-S-H rich melt which selectively elevated $(La/Yb)_N$ and PPGE ± Re abundances, as described above.

5.5 Comparisons of Kilbourne Hole peridotites with estimates of primitive mantle composition

The observation that large datasets derived from orogenic and xenolithic peridotites acknowledged to have experienced extensive metasomatism (e.g. Meisel et al., 2001; Becker et al., 2006; Wang et al., 2013), tend to project back to values for PUM suggests that the effects of metasomatism are not only widespread (König et al., 2014), but also may be included in estimates for HSE and chalcophile element abundances of PUM. Sample selection that takes into account metasomatism, which is apparent in lithophile, chalcophile and siderophile element systematics, should be critical in this respect. Estimates of PUM HSE and chalcophile element abundances have, to date, relied upon compilations of orogenic peridotite and xenolithic peridotite projected back to a major element composition consistent with zero melt extraction (Meisel et al., 2001; Becker et al., 2006) and interpreted with respect to chondritic abundances (Horan et al., 2003; Lodders et al., 2009). For this method to

831 successfully predict PUM abundances requires careful selection of samples so as to exclude
832 peridotites that do not best reflect the influence of melt depletion.

833 Suprachondritic Pd/Ir (or Pd/Pt) and Ru/Ir in fertile mantle peridotites have been
834 widely reported from different tectonic settings (e.g., Pattou et al., 1996; Rehkämper et al.,
835 1999; Schmidt et al., 2000; Becker et al., 2006; Liu et al., 2009). One possible explanation for
836 this observation is that existing estimates for HSE and strongly siderophile element
837 abundances in PUM, based upon estimates from a wide range of orogenic and xenolithic
838 peridotites, are not accurate and / or the projection back to a PUM composition has been
839 made with inappropriate samples or methods. Although some of the potential problems in
840 using Al_2O_3 as a suitable melt depletion indicator could be overcome by using S, the
841 perturbations to sulfur abundances by supergene weathering, and evidence for the addition
842 and removal of sulfide in groups 1 and 2 respectively of this study do not make S a reliable
843 proxy for Al_2O_3. In fact, although plots of S versus Ir, Pd and Pt superficially resemble melt
844 depletion curves (Figure 11a, b and c, respectively), the knowledge that S and HSE
845 systematics have likely been disturbed in many of these xenoliths, and the lack of any strong
846 co-variation between Al_2O_3 and S (Figure 4a) suggests that these can only be regarded as
847 apparent melt depletion curves.

848 Historical estimates of the PUM composition (Meisel et al., 2001; Becker et al., 2006;
849 Wang et al., 2013) have employed peridotites that have been experienced BMS and Se-Te-
850 HSE metasomatism (Lorand et al., 2010; 2013; Alard et al., 2011). While xenolithic
851 peridotite is prone to the loss of Os and S (± Se) as a result of supergene weathering, the
852 remaining HSE in peridotite xenoliths are probably as reliable an indicator of mantle
853 processes as those abundances found in orogenic peridotites. For example, the co-variations
854 observed in the Kilbourne Hole xenoliths of this study between S and Ir, Pd and Pt (Figure
855 11a, b and c, respectively) fall within the range of values used in the literature to project back

856 to a PUM composition. In this study, the addition of metasomatic sulfides in the group 2
857 peridotites and removal of sulfide by a S-undersaturated melt have both been identified, yet
858 their compositions are indistinguishable from the orogenic and xenolithic peridotites reported
859 in the literature (Figure 11a, b and c). The inference from this observation is that, with the
860 exception of [Os] ($^{187}Os/^{188}Os$ is unlikely to be fractionated by supergene weathering),
861 peridotite xenoliths in general, and from Kilbourne Hole specifically, are as suitable a proxy
862 for calculating PUM HSE abundances as orogenic peridotites which have probably
863 experienced the same processes identified in this study, whether they were reported in prior
864 investigations of different localities or not. The observation that group 1 peridotites from this
865 study have experienced a loss of sulfide, yet still plot within the range of literature values
866 used to calculate PUM, suggest that the literature database of peridotite HSE abundances also
867 contains a considerable proportion of samples where HSE abundances have been diluted,
868 irrespective of whether they are xenoliths or from orogenic massifs.

869 With respect to the strongly chalcophile elements Se and Te, these elements also need
870 to be subjected to the same scrutiny as the lithophile and highly siderophile elements in
871 appraising the suitability of orogenic peridotites and peridotite xenoliths for making estimates
872 of PUM composition. König et al. (2014) recently discussed the merits of using both
873 orogenic peridotites and kimberlite-derived peridotite xenoliths to investigate the primitive
874 Se-Te systematics of pristine, undepleted mantle and concluded that neither Se–Te
875 concentrations, nor their relatively low and near-chondritic Se/Te ratios can be considered as
876 primitive features of the Earth's mantle. Although this standpoint was subsequently
877 challenged (Wang and Becker, 2015a), the mineral-scale Se/Te study of König et al. (2015a)
878 that followed, in addition to the clarification of their earlier hypothesis (König et al., 2015b),
879 suggest that chondritic Se/Te and Se-Te concentrations seem unlikely to represent primitive
880 mantle. Selenium concentrations in Kilbourne Hole peridotites are low and project to around

881 50% of the concentration of PUM (McDonough and Sun, 1995), and consequently possess
882 lower Se/Te ratios than many of the literature values reported by Lorand et al. (2010, 2012),
883 Alard et al. (2011), König et al. (2012, 2014) and Wang et al. (2013) (Figure 5c). Despite
884 careful study of the multiphase petrogenetic history of Kilbourne Hole lherzolites, the nature
885 of the Se systematics of PUM remains equivocal. What is obvious is that the literature
886 compilation of Se-Te data that trend towards the Primitive Mantle and chondritic estimates of
887 McDonough and Sun (1995) and Palme and Jones (2003) respectively, contain many samples
888 that possess Se abundances in excess of that predicted for PUM. Although the large degree of
889 scatter of Se abundances amongst the Kilbourne Hole peridotites and the likelihood of Se loss
890 during transport of the xenoliths to the surface makes it difficult to quantify what the effects
891 of melt depletion on Se abundances were in these peridotites, any projection to a PUM-like
892 Se abundance using these peridotites alone would only underestimate the true PUM value.
893 The inclusion of peridotites with elevated Se abundances relative to PUM to estimate PUM
894 itself suggests that the current estimate of Se abundance in PUM is too high. Perhaps a more
895 realistic value for Se in PUM lies somewhere inbetween these estimates. Alternatively, high
896 Te abundances could skew the observed Se/Te systematics of the Kilbourne Hole peridotites.
897 In KH03-7 from this study (cf. UM9 of Morgan, 1986) an unusually high Te concentration
898 was detected that was not replicated in a second measurement. This hints at a particularly
899 intense nugget effect possibly caused by Te-rich micro-phases (Lorand et al., 2013; König et
900 al., 2014). This phenomenon may also explain the particularly high Pt concentration observed
901 in KH96-24, albeit without an anomalous Te abundance. In this respect the Kilbourne Hole
902 xenoliths have no more an unusual range of Te abundances than the orogenic peridotites used
903 for PUM calculations and it seems more likely that low Se abundances in these xenoliths
904 result in the Se/Te ratios that plot below any plausible melt depletion trend (Figure 12).

Perhaps this is more compelling evidence for the mobility of Se as a result of supergene weathering.

6. Concluding remarks

This study represents the first instance where Se-Te-HSE systematics in peridotite xenoliths are scrutinized in detail in order to test their usefulness for PUM estimates. Melt-impregnated or metasomatized peridotites may not be the best tools for estimating the HSE and chalcophile element composition of PUM; neither orogenic peridotites nor carefully screened peridotite xenoliths appear to offer unequivocal solutions as to the composition of their melt depleted pre-cursor. There are problems in estimating HSE and chalcophile element abundances from worldwide peridotite datasets that have not been adequately screened for subtle effects of metasomatism or melt / rock interaction, and the Kilbourne Hole peridotites of this study demonstrate that unequivocal values for PUM composition with regard to HSE, Se and Te concentrations are unlikely to be derived from peridotite xenoliths. It is only by selecting peridotites that have been scrupulously scrutinized for the effects of processes other than melt depletion that accurate PUM abundances may be determined.

New evidence for Se being affected by secondary processes can be found in Kilbourne Hole peridotite xenoliths which in turn lowers the Se/Te in basalt-borne xenolithic peridotites to subchondritic values. This contrasts with recent reportedly chondritic Se/Te in kimberlite-borne peridotite xenoliths.

Acknowledgements

JH was supported by Natural Environment Research Council Grants NER/A/S/2001/00538 and NE/J017981/1. SK acknowledges funding from the German Research Foundation (DFG

930 grant KO40501-1/2). AL thanks the European Research Council for financial support (ERC
931 research grant 258558 "Early Earth"). The authors thank Moritz Lissner for his help with the
932 Se-Te-HSE analyses and Nick Marsh (University of Leicester) for assistance with the S
933 abundance measurements. We are grateful for thorough and thoughtful reviews from Lucáš
934 Ackerman, and two anonymous reviewers, and for the considerate and patient editorial
935 handling of Richard Walker which helped us considerably in improving this contribution.
936
937
938
939
940
941
942
943
944
945
946
947 **References**
948
949 Ackerman, L., Walker, R. J., Puchtel, I. S., Pitcher, L., Jelnek, E., Strnad, L. 2009. Effects of
950 melt percolation on highly siderophile elements and Os isotopes in subcontinental
951 lithospheric mantle: a study of the upper mantle profile beneath Central Europe.
952 Geochim. Cosmochim. Acta 73, 2400–2414. doi:10.1016/j.gca.2009.02.002.
953 Ackerman, L., Pitcher, L., Strnad, L., Puchtl, I. S., Jelínek, E., Walker, R. J., Rohovec, J.
954 2013. Highly siderophile element geochemistry of peridotites and pyroxenites from

955 Horní Bory, Bohemian Massif: Implications for HSE behaviour in subduction-related
956 upper mantle. Geochim. Cosmochim. Acta 100, 158-175.
957 http://dx.doi.org/10.1016/j.gca.2012.09.050.
958 Alard, O., Griffin, W. L., Lorand, J. P., Jackson, S., O'Reilly, S. R. 2000. Non-chondritic
959 distribution of highly siderophile elements in mantle sulfide. Nature 407, 891–894.
960 Alard, O., Griffin, W. L., Pearson, N. J., Lorand J. - P., O'Reilly, S.Y. 2002. New insights
961 into the Re–Os systematics of subcontinental lithospheric mantle from in-situ analysis of
962 sulfides. Earth Planet. Sci. Lett. 203, 651–663.
963 Alard, O., Luguet, A., Pearson, N. J., Griffin, W. L., Lorand, J. - P., Gannoun, A., Burton, K.
964 W., O'Reilly, S. Y. 2005. In-situ Os isotopes in abyssal peridotites bridge the isotopic
965 gap between MORBs and their source mantle. Nature 436, 1005–1008.
966 doi:10.1038/nature03902.
967 Alard, O., Lorand, J.-P., Reisberg, L., Bodinier, J.-L., Dautria, J.-M., O'Reilly, S.Y. 2011.
968 Volatile-rich metasomatism in Montferrier xenoliths (Southern France): Implications for
969 the abundances of chalcophile and highly siderophile elements in the subcontinental
970 mantle. J. Petrol. 52 (10), 2009-2045. doi:10.1093/petrology/egr038.
971 Andersen, T., O'Reilly, S. Y., Griffin, W. L. 1984. The trapped fluid phase in upper mantle
972 xenoliths from Victoria: implications for mantle metasomatism. Contrib. Mineral. Petrol.
973 88, 72-95.
974 Anthony, E. Y., Kappus, E., Velador, J. 2002. Rio Grande Rift lithospheric structure and age
975 as revealed by mantle xenoliths from Kilbourne Hole, New Mexico. Geol. Soc. Am.
976 Abstracts 34, A253.
977 Baker, M. D., Stolper, E. M. 1994. Determining the composition of high pressure melts using
978 diamond aggregates. Geochim. Cosmochim. Acta 58, 2811-2827.

979 Baker, M. D., Hirschmann, M. M., Ghiorso, M. S., Stolper, E. M. 1995. Composition of near
980 solidus peridotite melts from experiments and thermodynamic calculations. Nature 375,
981 308-311.
982 Ballhaus, C., Bockrath C., Wohlgemuth-Ueberwasser, C., Laurenz V., Berndt J. 2006.
983 Fractionation of the noble metals by physical processes. Contrib. Mineral. Petrol. 152,
984 667–684. doi 10.1007/s00410-006-0126-z.
985 Barnes, S., Naldrett, A., Gorton, M. 1985. The origin of the fractionation of platinum-group
986 elements in terrestrial magmas. Chem. Geol. 53, 303–323.
987 Barnes, S.- J., Makovicky, E., Karup-Moller, S., Makovicky, M., Rose-Hansen, J. 1997.
988 Partition coefficients for Ni, Cu, Pd, Pt, Rh and Ir between Monosulphide solid solution
989 and sulphide liquid and the implications for the formation of compositionally zoned Ni–
990 Cu sulphide bodies by fractional crystallization of sulphide liquid. Can. J. Earth Sci. 34,
991 366–374.
992 Batanova, V. G., Belousov, I. A., Savelieva, G. N., Sobolev A. V. 2011. Consequences of
993 channelized and diffuse melt transport in supra-subduction zone mantle: evidence from
994 the Voykar Ophiolite (Polar Urals). J. Petrol. 52, 2483–2521.
995 doi:10.1093/petrology/egr053.
996 Becker, H., Shirey, S. B., Carlson, R. W. 2001. Effects of melt percolation on the Re–Os
997 systematics of peridotites from a Paleozoic convergent plate margin. Earth Planet. Sci.
998 Lett. 188, 107–121.
999 Becker, H., Horan, M. F., Walker, R. J., Gao, S., Lorand, J.-P., Rudnick, R. L. 2006. Highly
1000 siderophile element compositions of the earth's primitive mantle. Geochim. Cosmochim.
1001 Acta 70, 4528–4550. doi:10.1016/j.gca.2006.06.004.

1002 Bedini, R. M., Bodinier, J. L., Dautria, J. M., Morten, L. 1997. Evolution of LILE-enriched
1003 small melt fractions in the lithospheric mantle: a case from the East African Rift. Earth
1004 Planet. Sci. Lett. 153, 67–83.
1005 Blundy, J., Wood, B. 1994. Prediction of crystal-melt partition coefficients from elastic
1006 moduli. Nature 372, 452-454.
1007 Blundy, J., Wood, B. 2003. Partitioning of trace elements between crystals and melts. Earth
1008 Planet. Sci. Lett. 210, 383-397. doi:10.1016/S0012-821X(03)00129-8.
1009 Bockrath, C., Ballhaus, C., Holzheid, A. 2004. Fractionation of the platinum group elements
1010 during mantle melting. Science 305, 1951–1953.
1011 Bodinier, J. - L., Vasseur, G., Vernières, J., Dupuy, C., Fabriès J. 1990. Mechanism of mantle
1012 metasomatism: geochemical evidence from the Lherz orogenic peridotite. J. Petrol. 31,
1013 597–628.
1014 Bodinier, J. - L., Godard, M. 2003. Orogenic, Ophiolitic, and Abyssal Peridotites. In:
1015 Carlson, R.W. (Ed.), The Mantle and Core. Treatise on Geochemistry, 2.04, 103-170.
1016 Elsevier, Amsterdam.
1017 Bodinier, J. – L., Menzies, M. A., Shimizu, N., Frey, F. A., McPherson, E. 2004. Silicate,
1018 Hydrous and Carbonate Metasomatism at Lherz, France: Contemporaneous Derivatives
1019 of Silicate Melt-Harzburgite Reaction. J. Petrol. 49(2) 299-320. doi:
1020 10.1093/petrology/egg107.
1021 Bodnar, R. J. 2003. Introduction to fluid inclusions. In: Samson, I., Ansderson, A., Marshall,
1022 D. (Eds.) Fluid inclusions, analysis and interpretation. Min. Assoc. Canada. Short Course
1023 Series 32, 213-230.
1024 Brenan, J. M. 2002. Re-Os fractionation in magmatic sulfide melt by monosulfide solid
1025 solution. Earth Planet. Sci. Lett. 199, 257-268.

1026 Brenan, J.M. 2008. Re–Os fractionation by sulfide melt–silicate melt partitioning: A new
1027 spin. Chem. Geol. 248, 140-165. doi:10.1016/j.chemgeo.2007.09.003.
1028 Brenan, J. M., McDonough, W. F., Dalpé, C. 2003. Experimental constraints on the
1029 partitioning of rhenium and some platinum-group elements between olivine and silicate
1030 melt. Earth Planet. Sci. Lett. 212, 135–150. doi:10.1016/S0012-821X(03)00234-6.
1031 Brenan, J. M., McDonough, W. F., Ash, R. 2005. An experimental study of the solubility and
1032 partitioning of iridium, osmium and gold between olivine and silicate melt. Earth Planet.
1033 Sci. Lett. 237, 855–872. doi:10.1016/j.epsl.2005.06.051.
1034 Brey, G. P., Kohler, T. 1990. Geothermobarometry in four phase spinel lherzolites II: A
1035 practical assessment of existing thermobarometers. J. Petrol. 31, 1353-1378.
1036 Büchl, A., Brügmann, G., Batanova, V. G., Münker, C., Hofmann, A. W. 2002. Melt
1037 percolation monitored by Os isotopes and HSE abundances: a case study from the mantle
1038 section of the Troodos Ophiolite. Earth Planet. Sci. Lett. 204, 385-402.
1039 Burnham, O. M., Rogers, N. W., Pearson, D. G., van Calsteren, P., Hawkesworth, C. J. 1998.
1040 The petrogenesis of the eastern Pyrrenian peridotites: an integrated study of their whole-
1041 rock geochemistry and Re–Os isotope composition. Geochim. Cosmochim. Acta 62,
1042 2293–2310.
1043 Burton, K. W., Schiano, P., Birck, J.-L., Allègre, C. J. 1999. Osmium isotope disequilibrium
1044 between mantle minerals in a spinel-lherzolite. Earth Planet. Sci. Lett. 172, 311–322.
1045 Burton, K. W., Cenki-Tok, B., Mokadem, F., Harvey, J., Gannoun, A., Alard, O., Parkinson,
1046 I. J. 2012. Unradiogenic lead in Earth's upper mantle. Nature Geoscience 5 (8), 570–573.
1047 doi: 10.1038/ngeo1531.
1048 Bussod, G. Y. A. 1981. Thermal and kinematic history of mantle xenoliths from Kilbourne
1049 Hole, New Mexico, MSc thesis, University of Washington, Seattle, 72 pp.

1050 Bussod, G. Y. A., Williams, D. R. 1991. Thermal and kinematic model of the southern Rio
1051 Grande rift: inferences from crustal and mantle xenoliths from Kilbourne Hole, New
1052 Mexico. Tectonophys. 197, 373–389.
1053 Cordell, L., Zorin, Y. A., Keller, G. R. 1991. The decompensative gravity anomaly and deep
1054 structure of the region of the Rio Grande rift. J. Geophys. Res. 96, 6557-6568.
1055 Dale, C. W., Luguet, A., Macpherson, C. G., Pearson, D. G., Hickey-Vargas, R. 2008.
1056 Extreme platinum-group element fractionation and variable Os isotope compositions in
1057 Philippine Sea Plate basalts: Tracing mantle source heterogeneity. Chem. Geol. 248,
1058 213-238. doi:10.1016/j.chemgeo.2007.11.007.
1059 Dale, C. W., Macpherson, C. G., Pearson, D. G., Hammond, S. J., Arculus, R. J. 2012. Inter-
1060 element fractionation of highly siderophile elements in the Tonga Arc due to flux
1061 melting of a depleted source. Geochim. Cosmochim. Acta 89, 202-225.
1062 http://dx.doi.org/10.1016/j.gca.2012.03.025.
1063 Dautria, J. M., Dupuy, C., Tahkerist, D., Dostal, J. 1992. Carbonate metasomatism in the
1064 lithospheric mantle: peridotitic xenoliths from a melilitic district of the Sahara Basin.
1065 Contrib. Mineral. Petrol. 111, 37-52.
1066 De Bièvre, P., Taylor P. D. P. 1993. Table of the isotopic composition of the elements. Int. J.
1067 Mass Spectrom. Ion Processes 123, 149–166.
1068 Decker, E. R., Smithson, S. B. 1975. Heat flow and gravity interpretation across the Rio
1069 Grande rift in southern New Mexico and west Texas. J. Geophys. Res. 80, 2542-2552.
1070 Delpech, G., Lorand, J. - P., Grégoire, M, O'Reilly, S. Y. 2012. In situ geochemistry of
1071 chalcophile and highly siderophile elements in highly metasomatized in Kergeulen
1072 mantle xenoliths (South Indian Ocean). Lithos 154, 296-314.
1073 doi:10.1016/j.lithos.2012.07.018.

1074 Dick, H. J. B., Lissenberg, C. J., Warren, J. M. 2010. Mantle melting, melt transport, and
1075 delivery beneath a slow-spreading ridge: the paleo-MAR from 23°15´N to 23°45´N. J.
1076 Petrol. 51, 425–467. doi: 10.1093/petrology/epg088.
1077 Dreibus, G., Palme, H., Spettel, B., Zipfel, J., Wanke, H. 1995. Sulfur and selenium in
1078 chondritic meteorites. Meteoritics 30, 439-445.
1079 Dromgoole, E. L., Pasteris, J. D. 1987. Interpretation of the sulfide assemblages in a suite of
1080 xenoliths from Kilbourne Hole, New Mexico. Geol. Soc. Am. Spec. Pap. 215, 25–46.
1081 Elton, D. 1992. Chemical trends in abyssal peridotites: refertilization of depleted sub oceanic
1082 mantle, J. Geophys. Res. 97 (B6) 9015–9025.
1083 Elwaer, N., Hintelmann, H. 2008. Selective separation of selenium (IV) by thiol cellulose
1084 powder and subsequent selenium isotope ratio determination using multicollector
1085 inductively coupled plasma mass spectrometry. J. Anal. At. Spectrom. 23(5), 733–743.
1086 doi: 10.1039/b801673a.
1087 Ferraris, C., Lorand, J. – P. 2008. HRTEM-AEM-HAADF-STEM study of platinum-group
1088 elements within a mantle-derived Cr spinel (Lherz; North-Eastern Pyrenees, France).
1089 Earth Planet. Sci. Lett. 276, 167-174. doi:10.1016/j.epsl.2008.09.019.
1090 Fischer-Gödde, M., Becker, H., Wombacher, F. 2010. Rhodium, gold and other highly
1091 siderophile element abundances in chondritic meteorites. Geochim. Cosmochim. Acta
1092 74, 356–379. doi: 10.1016/j.gca.2009.09.024.
1093 Fischer-Gödde, M., Becker, H., Wombacher, F. 2011. Rhodium, gold and other highly
1094 siderophile elements in orogenic peridotites and peridotite xenoliths. Chem. Geol. 280,
1095 365–383.
1096 Fleet, M. E., Stone, W. E., Crocket, J. H. 1991. Partitioning of palladium, iridium, and
1097 platinum between sulfide liquid and basalt melt: effects of melt composition,
1098 concentration and oxygen fugacity. Geochim. Cosmochim. Acta 55, 2545–2554.

1099 Fleet, M. E., Crocket, J. H., Stone, W. E. 1996. Partitioning of platinum group elements (Os,
1100 Ir, Ru, Pt, Pd) and gold between sulfide liquid and basalt melt. Geochim. Cosmochim.
1101 Acta 60, 2397–2412.
1102 Fleet, M. E., Crocket, J. H., Liu, M., Stone, W. E. 1999. Laboratory partitioning of platinum-
1103 group elements (PGE) and gold with application to magmatic sulfide- PGE deposits.
1104 Lithos 47, 127–144.
1105 Frey, F. A., Green, D. H. 1974. The mineralogy, geochemistry and origin of lherzolite
1106 inclusions in Victorian basanites. Geochim. Cosmochim. Acta 38, 1023–1059.
1107 Frost, D. J., McCammon, C. A. 2008. The redox state of Earth's mantle. Annu. Rev. Earth
1108 Planet. Sci. 36, 389–420. doi: 10.1146/annurev.earth.36.031207.124322.
1109 Galer, S. J. G., O'Nions, R. K. 1989. Chemical and isotopic studies of ultramafic inclusions
1110 from the San Carlos Volcanic Field, Arizona: a bearing on their petrogenesis. J. Petrol.
1111 30, 1033–1064.
1112 Griffin, W. L., Smith, D., Ryan, C. G., O'Reilly, S. Y., Win, T. T. 1996. Trace element
1113 zoning in mantle minerals: metasomatism and thermal events in the upper mantle. Canad.
1114 Mineral. 34, 1179-1193.
1115 Griffin, W. L., Spetsius, Z.V., Pearson, N. J., O'Reilly, S. Y. 2002. In situ Re–Os analysis of
1116 sulfide inclusions in kimberlitic olivine: new constraints on depletion events in the
1117 Siberian lithospheric mantle. Geochem. Geophys. Geosyst. 3(11), doi:10.1029/
1118 2001GC000287.
1119 Guo, J., Griffin, W. L., O'Reilly, S. Y. 1999. Geochemistry and origin of sulfide minerals in
1120 mantle xenoliths: Qilin, Southeastern China. J. Petrol. 40, 1125–1149.
1121 Handler, M. R., Bennett, V. C., 1999. Behaviour of Platinum-group elements in the
1122 subcontinental mantle of eastern Australia during variable metasomatism and melt
1123 depletion. Geochim. Cosmochim. Acta 63 (21), 3597-3618.

1124 Hart, S. R., Ravizza, G. 1996. Os partitioning between phases in lherzolite and basalt. In:
1125 Earth Processes: Reading the Isotopic Code (eds. A. Basu and S. R. Hart). Geophys.
1126 Mon., vol. 95. AGU, Washington. pp. 123–134.
1127 Harte, B. 1983. Mantle peridotite and processes – the kimberlite sample. In: Continental
1128 basalts and mantle xenoliths. (Eds Hawkesworth, C.J., Norry, M.J.) Shiva Publishing,
1129 Nantwich, UK. p.46.
1130 Harvey, J., Gannoun, A., Burton, K. W., Rogers, N. W., Alard, O., Parkinson, I. J. 2006.
1131 Ancient melt extraction from the oceanic upper mantle revealed by Re–Os isotopes from
1132 the Mid-Atlantic Ridge. Earth Planet. Sci. Lett. 244, 606–621.
1133 doi:10.1016/j.epsl.2006.02.031.
1134 Harvey J., Gannoun A., Burton K. W., Rogers N. W., Schiano P., Alard O. 2010. Unravelling
1135 the effects of melt depletion and secondary infiltration on mantle Re–Os isotopes beneath
1136 the French Massif Central. Geochim. Cosmochim. Acta 74, 293–320.
1137 doi:10.1016/j.gca.2009.09.031.
1138 Harvey, J., Dale, C. W., Gannoun, A., Burton, K. W. 2011. Osmium mass balance in
1139 peridotite and the effects of mantle-derived sulfides on basalt petrogenesis. Geochim.
1140 Cosmochim, Acta 75, 5574-5596. doi:10.1016/j.gca.2011.07.001.
1141 Harvey, J., Yoshikawa, M., Hammond, S. J., Burton, K. W. 2012. Deciphering the trace
1142 element characteristics in Kilbourne Hole peridotite xenoliths: melt-rock interaction and
1143 metasomatism beneath the Rio Grande Rift, SW USA. J. Petrol. 53 (8), 1709-1742.
1144 doi:10.1093/petrology/egs030.
1145 Hattori, K. H., Arai, S., Clarke, D. B. 2002. Selenium, tellurium, arsenic and antimony
1146 contents of primary mantle sulfides. Can. Mineral. 40, 637–650.
1147 Helmy, H. M., Ballhaus, C., Wohlgemuth-Ueberwasser, C., Fonseca, R. O. C., Laurenz,V.
1148 2010. Partitioning of Se, As, Sb, Te and Bi between monosulfide solid solution and

1149 sulfide melt–Application to magmatic sulfide deposits. Geochim. Cosmochim. Acta 74,
1150 6174–6179, doi:10.1016/j.gca.2010.08.009.
1151 Hertogen, J., Janssens, M. J., Palme, H. 1980. Trace elements in ocean ridge basalt glasses:
1152 implications for fractionations during mantle evolution and petrogenesis. Geochim.
1153 Cosmochim. Acta 44, 2125–2143.
1154 Hirschmann, M. M., Baker, M. B., Stolper, E. M. 1998. The effect of alkalis on the silica
1155 content of mantle-derived melts. Geochim. Cosmochim. Acta 5, 883-902.
1156 Hoffer, J. M. 1976. The Potrillo basalt field, south-central New Mexico. In: Elston,W. and
1157 Northrop, S. A. (eds) Cenozoic Volcanism in Southwestern New Mexico. New Mexico
1158 Geol. Soc. Spec. Pub. 5, 89-92.
1159 Holzheid, A. 2010. Separation of sulfide melt droplets in sulfur saturated silicate liquids.
1160 Chem. Geol. 274, 127–135. doi:10.1016/j.chemgeo.2010.03.005.
1161 Horan, M. F., Walker, R. J., Morgan, J. W., Grossman, J. N., Rubie, A. E. 2003. Highly
1162 siderophile element in chondrites. Chem. Geol. 196, 5–20. doi:10.1016/S0009-
1163 2541(02)00405-9.
1164 Ionov, D. A., Dupuy, C., O'Reilly, S. Y., Kopylova, M. G., Genschaft, Y. S. 1993.
1165 Carbonated peridotite xenoliths from Spitzbergen: implications for the trace element
1166 signature of mantle carbonate metasomatism. Earth Planet. Sci. Lett. 119, 283-297.
1167 Ionov, D. A., Shirey, S. B., Weis, D., Brügmann, G. 2006. Os–Hf–Sr–Nd isotope and PGE
1168 systematics of spinel peridotite xenoliths from Tok, SE Siberian craton: effects of
1169 pervasive metasomatism in shallow refractory mantle. Earth Planet. Sci. Lett. 241, 47–
1170 64. doi:10.1016/j.epsl.2005.10.038.
1171 Jagoutz E., Palme H., Blum H., Cendales M., Dreibus G., Spettel, B., Lorenz V., Wänke H.
1172 1979. The abundances of major, minor and trace elements in the Earth's mantle as

derived from primitive ultramafic nodules. Proceedings of 10th LPSC. Geochim. Cosmochim. Acta Suppl. 10, 2031–2051.

Keller, G. R., Morgan, P., Seager, W. R. 1990. Crustal structure, gravity anomalies and heat flow in the southern Rio Grande rift and their relationship to extensional tectonics. Tectonophys. 174, 21-37.

Kil, Y., Wendlandt, R. F. 2004. Pressure and temperature evolution of upper mantle under the Rio Grande rift. Contrib. Mineral. Petrol. 148, 2665-2680. doi:10.1007/s00410-004-0608-9.

König, S., Luguet, A., Lorand, J. - P., Wombacher, F., Lissner, M. 2012. Selenium and tellurium systematics of the Earth's mantle from high precision analyses of ultra depleted orogenic peridotites. Geochim. Cosmochim. Acta 86, 354–366. http://dx.doi.org/10.1016/j.gca.2012.03.014.

König, S., Lorand, J. - P., Luguet, A., Pearson, D. G. 2014. A non-primitive origin of near-chondritic S–Se-Te ratios in mantle peridotites; implications for the Earth's late accretionary history. Earth Planet. Sci. Lett. 385, 100-121. http://dx.doi.org/10.1016/j.epsl.2013.10.036.

König, S., Lissner, M., Lorand, J. - P., Bragagni, A., Luguet, A. 2015a. Mineralogical control of selenium, tellurium and highly siderophile elements in the Earth's mantle: Evidence from mineral separates of ultra-depleted mantle residues. Chem. Geol. 396, 16-24. http://dx.doi.org/10.1016/j.chemgeo.2014.12.015.

König, S., Luguet, A., Lorand, J. - P., Lissner, M., Pearson, D. G. 2015b. Reply to the comment on "A non-primitive origin of near-chondritic S–Se–Te ratios in mantle peridotites: Implications for the Earth's late accretionary history" by König S. et al. [Earth Planet. Sci. Lett. 385(2014) 110–121]. Earth Planet. Sci. Lett. 417, 167-169. http://dx.doi.org/10.1016/j.epsl.2015.02.032.

1198 Kogiso, T., Suzuki, K., Suzuki, T., Shinotsuka, K., Uesugi, K., Takeuchi, A., Suzuki, Y.
1199 2008. Detecting micrometer-scale platinum-group minerals in mantle peridotite with
1200 microbeam synchrotron radiation X-ray fluorescence analysis. Geochem., Geophys,
1201 Geosys 9, Q03018. http://dx.doi.org/10.1029/2007GC001888, 2008.
1202 Le Roux, V., Bodinier, J. - L., Tommasi, A., Alard, O., Dautria, J. - M., Vauchez, A., Riches,
1203 A. J. V. 2007. The Lherz spinel lherzolite: Refertilized rather than pristine mantle. Earth
1204 Planet. Sci. Lett. 259, 599-612. doi:10.1016/j.epsl.2007.05.026.
1205 Le Roux, V., Tommasi, A., Vauchez A. 2008. Feedback between melt percolation and
1206 deformation in an exhumed lithosphere‐asthenosphere boundary. Earth Planet. Sci. Lett.
1207 274(3–4), 401–413. doi:10.1016/j.epsl.2008.07.053.
1208 Le Roux, V., Bodinier, J.-L., Alard O., O'Reilly, S. Y., Griffin W. L. 2009. Isotopic
1209 decoupling during porous melt flow: a case study in the Lherz peridotite. Earth Planet.
1210 Sci. Lett. 279(1–2), 76–85. doi:10.1016/j.epsl.2008.12.033.
1211 Lissner, M., König, S., Luguet, A., le Roux, P.J., Schuth, S., Heuser, A., le Roex, A.P. 2014.
1212 Selenium and Tellurium systematics in MORBs from the southern Mid-Atlantic Ridge
1213 (47–50◦S). Geochim. Cosmochim. Acta144, 379–402.
1214 Liu, C. Z., Snow, J. E., Brügmann, G., Hellebrand, E., Hofmann A. W. 2009. Non-chondritic
1215 HSE budget in Earth's upper mantle evidenced by abyssal peridotites from Gakkel ridge
1216 (Arctic Ocean). Earth Planet. Sci. Lett. 283, 122–132.
1217 Lodders, K., Palme, H., Gail, H. P. 2009. Abundances of the elements in the solar system. In:
1218 Trumper, J. E. (Ed.), Landolt-Bornstein, New Series VI/4B(4.4), pp.560–630.
1219 Lorand, J.P. 1990. Are spinel lherzolite xenoliths representative of the sulfur content of the
1220 upper mantle. Geochim. Cosmochim. Acta 54, 1487–1492.

1221 Lorand, J. - P., Alard, O. 2001. Platinum-group element abundances in the upper mantle: new
1222 constraints from in-situ and whole-rock analyses of Massif Central xenoliths (France).
1223 Geochim. Cosmochim. Acta 65, 2789–2806.
1224 Lorand, J. - P., Alard, O. 2010. Determination of selenium and tellurium concentrations in
1225 Pyrenean peridotites (Ariège, France): new insight into S/Se/Te systematics of the upper
1226 in mantle samples. Chem. Geol. 278(1-2), 120-130. doi:10.1016/j.chemgeo.2010.09.007.
1227 Lorand, J. - P., Gros, M., Pattou, L. 1999. Fractionation of platinum-group elements in the
1228 upper mantle: a detailed study in Pyrenean orogenic peridotites. J. Petrol. 40, 951–987.
1229 Lorand, J. - P., Schmidt, G., Palme, H., Kratz, K. L. 2000. Highly siderophile element
1230 geochemistry of the Earth's mantle: new data for the Lanzo (Italy) and Ronda (Spain)
1231 orogenic peridotite bodies. Lithos 53, 149–164.
1232 Lorand, J. - P., Alard, O., Luguet, A., Keays, R. R. 2003a. Sulfur and selenium systematics of
1233 the subcontinental lithospheric mantle: Inferences from the Massif Central xenolith suite
1234 (France). Geochim. Cosmochim. Acta 67 (21), 4137-4151. doi:10.1016/S0016-
1235 7037(00)00305-3.
1236 Lorand, J. - P., Reisberg, L., Bedini, R. M. 2003b. Platinum-group elements and melt
1237 percolation processes in Sidamo spinel peridotite xenoliths, Ethiopia, East African Rift.
1238 Chem. Geol. 196, 57–75. doi:10.1016/S0009-2541(02)00407-2.
1239 Lorand, J. - P., Delpech, G., Grégoire, M., Moine, B., O'Reilly, S. Y., Cottin, J. - Y. 2004.
1240 Platinum group elements and the multistage metasomatic history of Kerguelen
1241 lithospheric mantle South Indian Ocean. Chem. Geol. 208, 195–215.
1242 doi:10.1016/j.chemgeo.2004.04.012.
1243 Lorand, J. - P., Luguet, A., Alard, O., Bézos, A., Meisel, T. 2008. Distribution of platinum
1244 group elements in orogenic lherzolites: a case study in a Fontête Rouge lherzolite,
1245 (French Pyrenees). Chem. Geol. 248, 174–194. doi:10.1016/j.chemgeo.2007.06.030.

1246 Lorand, J. - P., Alard, O., Luguet, A. 2010. Platinum-group element micronuggets and
1247 refertilization process in Lherz orogenic peridotite (northeastern Pyrenees, France). Earth
1248 Planet. Sci. Lett. 289, 298-310. doi:10.1016/j.epsl.2009.11.017.
1249 Lorand, J. - P., Luguet, A., Alard, O. 2013. Platinum-group element systematics and
1250 petrogenetic processing of the continental upper mantle: A review. Lithos 164, 2–21.
1251 http://dx.doi.org/10.1016/j.lithos.2012.08.017.
1252 Luguet, A., Lorand, J. - P. 1998. Supergene weathering and sulfur contents of basalt-hosted
1253 mantle xenoliths: An appraisal from Montferrier lherzolites (Languedoc, France). C. R.
1254 Acad. Sci. Paris 327, 519–525.
1255 Luguet, A., Alard, O., Lorand, J. - P., Pearson, N. J., Ryan, C., O'Reilly, S. Y. 2001. Laser
1256 ablation microprobe (LAM)-ICPMS reveals the highly siderophile element geochemistry
1257 of the oceanic mantle. Earth Planet. Sci. Lett. 189, 285–294.
1258 Luguet, A., Lorand, J. P., Seyler, M. 2003. Sulfide petrology and highly siderophile element
1259 geochemistry of abyssal peridotites: A coupled study of samples from the Kane Fracture
1260 Zone (45°W, 23°20N, MARK Area, Atlantic Ocean). Geochim. Cosmochim. Acta 67,
1261 1553-1570.
1262 Luguet, A., Lorand, J .- P., Alard, O., Cottin, J.-Y. 2004. A multi-technique study of platinum
1263 group element systematic in some Ligurian ophiolitic peridotites, Italy. Chem. Geol. 208,
1264 175–194. doi:10.1016/j.chemgeo.2004.04.011.
1265 Luguet, A., Shirey, S., Lorand, J. - P., Horan, M. F., Carlson, R. C. 2007. Residual platinum
1266 group minerals from highly depleted harzburgites of the Lherz massif (France) and their
1267 role in HSE fractionation of the mantle. Geochim. Cosmochim. Acta 71, 3082–3097.
1268 doi:10.1016/j.gca.2007.04.011.
1269 Marchesi, C., Garrido, C. J., Harvey, J., González-Jiménez, J. - M., Hidas, K., Lorand, J. – P.,
1270 Gervilla, F. 2013. Platinum-group elements, S, Se and Cu in highly depleted abyssal

peridotites from the Mid-Atlantic Ocean Ridge (ODP Hole 1274A): Influence of hydrothermal and magmatic processes. Contrib. Mineral. Petrol. 166, 1521-1538. doi:10.1007/s00410-013-0942-x.

Marin, L., Lhomme, J., Carignan J. 2001. Determination of selenium concentration in sixty five reference materials for geochemical analysis by GFAAS after separation with thiol cotton. Geostandards Newslett.: J. Geostand. Geoanal. 25(2–3), 317–324.

Mavrogenes, J., O'Neill, H.St.C. 1999. The relative effects of pressure, temperature and oxygen fugacity on the solubility of sulfide in mafic magmas. Geochim. Cosmochim Acta 63, 1173–1180.

McDonough, W. F., Sun, S. S. 1995. The composition of the Earth. Chem. Geol. 120, 223-253.

Meisel, T., Moser, J. 2004. Reference materials for geochemical PGE analysis: new analytical data for Ru, Rh, Pd, Os, Ir, Pt and Re by isotope dilution ICP-MS in 11 geological reference materials. Chem. Geol. 208, 319–338. doi:10.1016/j.chemgeo.2004.04.019.

Meisel T., Walker R. J., Irving A. J., Lorand J. - P. 2001. Osmium isotopic compositions of mantle xenoliths: a global perspective. Geochim. Cosmochim. Acta 65, 1311–1323.

Meisel, T., Reisberg, L., Moser, J., Carignan, J., Melcher, F., Brügmann, G. 2003. Re–Os systematics of UB–N, a serpentinized peridotite reference material. Chem. Geol. 201, 161–179. doi:10.1016/S0009-2541(03)00234-1.

Menzies, M. A., Dupuy, C., 1991. Orogenic massifs: protolith, process and provenance. J. Petrol. 1–16 (Special Lithosphere Issue).

Menzies, M. A., Wass, S. Y. 1983. CO_2 and LREE rich mantle below eastern Australia: a rare earth and isotope study of alkaline magmas and apatite rich mantle xenoliths from the Southern Highlands Province, Australia. Earth Planet. Sci. Lett. 65, 287-302.

1296 Menzies, M. A., Arculus, R. J., Best, M. G., Bergman, S. C., Ehrenberg, S. N., Irving, A. J.,
1297 Roden, M. F., Schulze, D. J. 1987. A record of subduction process and within-plate
1298 volcanism in lithospheric xenoliths of the south-western USA. In: Nixon, P. N. (ed.)
1299 Mantle Xenoliths. Chichester: John Wiley, pp. 59-74.
1300 Moine, B. N., Grégoire, M., O'Reilly, S. Y., Delpech, G., Sheppard, S. M. F., Lorand, J. - P.,
1301 Renac, C., Giret, A., Cottin, J. Y. C. 2004. Carbonatite melt in oceanic upper mantle
1302 beneath the Kerguelen Archipelago. Lithos 75, 239–252. doi: 10.1016/j.lithos.2003.12.
1303 Morgan, J. W. 1986. Ultramafic xenoliths: Clues to Earth's late accretionary history. J.
1304 Geophys. Res. 91 (B12), 12375-12387.
1305 Morgan, J. W., Baedecker, P. A. 1983. Elemental composition of sulfide particles from an
1306 ultramafic xenolith and the siderophile element content of the upper mantle. Lunar and
1307 Planetary Science Conference XIV, pp. 513–514.
1308 Morgan, J. W., Walker, R. J., Brandon, A. D., Horan, M. F. 2001. Siderophile elements in the
1309 Earth's upper mantle and lunar breccias: data synthesis suggests manifestations of the
1310 same late influx. Meteorit. Planet. Sci. 36, 1257–1275.
1311 Mungall, J. E., Brenan, J. M. 2014. Partitioning of platinum-group elements and Au between
1312 sulfide liquid and basalt and the origins of mantle-crust fractionation of the chalcophile
1313 elements. Geochim. Cosmochim. Acta 125, 265-289.
1314 http://dx.doi.org/10.1016/j.gca.2013.10.002.
1315 Müntener, O., Pettke, T., Desmurs, L., Meier, M., Schaltegger, U. 2004. Refertilisation of
1316 mantle peridotite in embryonic ocean basins: trace element and Nd isotopic evidence and
1317 implications for crust-mantle relationships. Earth Planet. Sci. Lett. 221, 293–308.
1318 doi:10.1016/S0012-821X(04)00073-1.
1319 Navon, O., Stolper, E. M. 1987. Geochemical consequences of melt percolation: the upper
1320 mantle as a chromatographic column. J. Geology 95, 285-308.

1321 O'Driscoll, B., Day, J. M. D., Walker, R. J., Daly, J. S., McDonough, W. F., Piccoli, P. M.
1322 2012. Chemical heterogeneity in the upper mantle recorded by peridotites and
1323 chromitites from the Shetland Ophiolite Complex, Scotland. Earth Planet. Sci. Lett. 333-
1324 334, 226-237. http://dx.doi.org/10.1016/j.epsl.2012.03.035.
1325 Olsen, K. H., Morgan, P. 1995. Introduction: progress in understanding continental rifts. In:
1326 Olsen, K. H. (ed.) Continental Rifts: Evolution, Structure and Tectonics. Developments
1327 in Geotectonics 25, 3-26.
1328 O'Neill, H. St. C. 1991. The origin of the moon and the early history of the Earth—a
1329 chemical model: Part 2. The Earth. Geochim. Cosmochim. Acta 55, 1159–1172.
1330 O'Neill, H. St. C., Mavrogenes, J. 2002. The sulfide capacity and the sulfur content at sulfide
1331 saturation of silicate melts at 1400 C and 1 bar. J. Petrol. 43(6), 1049-1087.
1332 O'Reilly, S. Y., Griffin, W. L. 1988. Mantle metasomatism beneath western Victoria,
1333 Australia: (I) metasomatic processes in Cr-diopside lherzolites. Geochim. Cosmochim.
1334 Acta 52, 433-447.
1335 Palme, H., Jones, A. 2003. Solar system abundances of the elements. In: Carlson, R.W. (Ed.),
1336 The Mantle and Core. Treatise on Geochemistry. Elsevier, Amsterdam, pp 41-61.
1337 Palme, H., O'Neill, H. St. C. 2003. Cosmochemical estimates of mantle composition. In:
1338 Carlson, R.W. (Ed.), The Mantle and Core. Treatise on Geochemistry. Elsevier,
1339 Amsterdam, pp. 1–38.
1340 Pattou, L., Lorand, J. - P., Gros, M. 1996. Non-chondritic platinum-group element ratios in
1341 the Earth's mantle. Nature 379, 712–715.
1342 Peach, C. L., Mathez, E. A. 1993. Sulfide melt-silicate melt distribution coefficients for
1343 nickel and iron and implications for the distribution of other chalcophile elements.
1344 Geochim. Cosmochim. Acta 57, 3013-3021.

1345 Peach, C. L., Mathez, E. A., Keays, R. R. 1990. Sulfide melt–silicate melt distribution
1346 coefficients for noble metals and other chalcophile elements as deduced from MORB:
1347 implications for partial melting. Geochim. Cosmochim. Acta 54, 3379–3389.
1348 Peach, C. L., Mathez, E. A., Keays, R. R., Reeves, S. J. 1994. Experimentally determined
1349 sulfide melt–silicate melt partition coefficients for iridium and palladium. Chem. Geol.
1350 117, 361-377.
1351 Pearson, D. G., Woodland, S. J. 2000. Solvent extraction/anion exchange separation and
1352 determination of PGE (Os, Ir, Pt, Pd, Ru) and Re–Os isotopes in geological samples by
1353 isotope dilution ICP-MS. Chem. Geol. 165, 87–107.
1354 Pearson, D. G., Irvine, G. J., Ionov, D. A., Boyd, F. R., Dreibus, D. E. 2004. Re–Os isotope
1355 systematics and platinum group element fractionation during mantle melt extraction: a
1356 study of massif and xenolith peridotite suites. Chem. Geol. 208, 29-59.
1357 doi:10.1016/j.chemgeo.2004.04.005.
1358 Peregoedova, A., Barnes, S. –J., Baker, D. R. 2004. The formation of Pt-Ir alloys and Cu-Pd-
1359 rich sulfide melts by partial desulfurization of Fe-Ni-Cu sulfides: results of experiments
1360 and implications for natural systems. Chem. Geol. 208, 247–264.
1361 Piccardo, G. B., Zanetti, A., Müntener, O. 2007. Melt/peridotite interaction in the Southern
1362 Lanzo peridotite: field, textural and geochemical evidence. Lithos 94, 181–209.
1363 doi:10.1016/j.lithos.2006.07.002.
1364 Rehkämper, M., Halliday, A. N., Alt, J., Fitton, J. G., Zipfel, J., Takazawa, E. 1999. Non-
1365 chondritic platinum-group element ratios in oceanic mantle lithosphere: petrogenetic
1366 signature of melt percolation? Earth Planet. Sci. Lett. 172, 65–81.
1367 Reisberg, L., Lorand, J. P. 1995. Longevity of sub-continental mantle lithosphere from
1368 osmium isotope systematics in orogenic peridotite massifs. Nature 376, 159–162.

1369 Reisberg, L., Lorand, J. – P., Bedini, R.M. 2004. Reliability of Os model ages in pervasively
1370 metasomatized continental mantle lithosphere: a case study of Sidamo spinel peridotite
1371 xenoliths (East African Rift, Ethiopia). Chem. Geol. 208, 119-140.
1372 doi:10.1016/j.chemgeo.2004.04.008.
1373 Reisberg, L., Zhi, X., Lorand, J. – P., Wagner, C., Peng, Z., Zimmermann, C. 2005. Re–Os
1374 and S systematics of spinel peridotite xenoliths from east central China: Evidence for
1375 contrasting effects of melt percolation. Earth Planet. Sci. Lett. 239, 286-308.
1376 doi:10.1016/j.epsl.2005.09.010.
1377 Reiter, M., Eggleston, R. E., Broadwell, B. R., Minier, J. 1986. Estimates of terrestrial heat
1378 flow: deep petroleum tests along the Rio Grande rift in central and southern New
1379 Mexico. J. Geophys. Res. 91, 6225-6242.
1380 Riches, A. J. V., Rogers, N. W. 2011. Mineralogical and geochemical constraints on the
1381 shallow origin, ancient veining and multi-stage modification of the Lherz peridotite.
1382 Geochim. Cosmochim. Acta 75, 6160–6182. doi:10.1016/j.gca.2011.07.036.
1383 Righter, K., Campbell, A. J., Humayun, M., Hervig, R. L. 2004. Partitioning of Ru, Rh, Pd,
1384 Re, Ir, and Au between Cr-bearing spinel, olivine, pyroxene and silicate melts. Geochim.
1385 Cosmochim. Acta 68, 867–880.
1386 Robinson, J. A. C., Wood, B. J., Blundy, J. D. 1998. The beginning of melting of fertile and
1387 depleted peridotite at 1·5 GPa. Earth Planet. Sci. Lett. 155, 97-111.
1388 Roden, M. F., Frey, F. A., Francis, D. 1984. An example of consequent mantle metasomatism
1389 in peridotite inclusions from Nunivak Island, Alaska. J. Petrol. 25, 547-577.
1390 Rudnick, R. L., McDonough, W. F., Chappell, B. W. 1993. Carbonatite metasomatism in the
1391 northern Tanzanian mantle: petrographic and geochemical characteristics. Earth Planet.
1392 Sci. Lett. 114, 463-475.

1393 Savard, D., Bédard, L. P., Barnes, S.-J. 2009. Selenium concentrations in twenty-six
1394 geological reference materials: new determinations and proposed values. Geostand.
1395 Geoanal. Res. 33(2), 249–259.
1396 Schiano, P., Bourdon, B. 1999. On the preservation of mantle information in ultramafic
1397 nodules: glass inclusions within minerals versus interstitial glass. Earth. Planet. Sci. Lett.
1398 169,173-188.
1399 Schiano, P., Clocchiatti, R. 1994. Worldwide occurrence of silica-rich melts in sub-oceanic
1400 and sub-continental mantle minerals. Nature 368, 621-624.
1401 Schmidt, G., Palme, H., Kratz, K. L., Kurat G. 2000. Are highly siderophile elements (PGE,
1402 Re and Au) fractionated in the upper mantle of the earth? New results on peridotites from
1403 Zabargad. Chem. Geol. 163, 167–188.
1404 Seyler, M., Toplis, M. J., Lorand, J. – P., Luguet, A., Cannat, M. 2001. Clinopyroxene
1405 microtextures reveal incompletely extracted melts in abyssal peridotites. Geology 29 (2),
1406 155-158.
1407 Seyler, M., Lorand, J. – P., Dick, H. B. J., Drouin, M. 2007. Pervasive melt percolation
1408 reactions in ultra-depleted refractory harzburgites at the Mid-Atlantic Ridge, 15°20'N:
1409 ODP Hole 1274A. Contrib. Mineral. Petrol. 153, 303-319. doi 10.1007/s00410-006-
1410 0148-6.
1411 Soustelle, V., Tommasi, A., Bodinier., J. - L., Garrido, C. J., Vauchez, A. 2009. Deformation
1412 and reactive melt transport in the mantle lithosphere above a large-scale partial melting
1413 domain: the Ronda peridotite massif, Southern Spain. J. Petrol. 50, 1235-1266.
1414 doi:10.1093/petrology/egp032.
1415 Terashima, S. 2001. Determination of indium and tellurium in fifty nine geological reference
1416 materials by solvent extraction and graphite furnace atomic absorption spectrometry.
1417 Geostandards Newslett.: J. Geostand. Geoanal. 25(1), 127–132.

1418 Terashima, S., Imai, N. 2000. Determination of selenium in fifty two geochemical reference
1419 materials by hydride generation atomic absorption spectrometry. Geostandards
1420 Newslett.: J. Geostand. Geoanal. 24(1), 83–86.
1421 Thompson, R. N., Ottley, C. J., Smith, P. M., Pearson, D. G., Dickin, A. P., Morrison, M. A.,
1422 Leat, P. T., Gibson, S. A. 2005. Source of the Quaternary alkalic basalts, picrites and
1423 basanites of the Potrillo volcanic field, New Mexico, USA: lithosphere or convecting
1424 mantle? J. Petrol. 46, 1603–1643. doi:10.1093/petrology/egi028.
1425 van Acken, D., Becker, H., Walker, R. J. 2008. Refertilization of Jurassic oceanic peridotites
1426 from the Tethys Ocean – implications for the Re–Os systematics of the upper mantle.
1427 Earth Planet. Sci. Lett. 268, 171–181. doi:10.1016/j.epsl.2008.01.002.
1428 van Acken, D., Becker, H., Hammerschmidt, K., Walker, R. J., Wombacher, F. 2010a.
1429 Highly siderophile elements and Sr–Nd isotopes in refertilised mantle peridotites–a case
1430 study from the Totalp ultramafic body, Swiss Alps. Chem. Geol. 276 (3–4), 257–268.
1431 doi:10.1016/j.gca.2009.10.007.
1432 van Acken, D., Becker, H., Walker, R. J., McDonough, W. F., Wombacher, F., Ash, R. D.,
1433 Piccoli P. M. 2010b. Formation of pyroxenite layers in the Totalp ultramafic massif
1434 (Swiss Alps) - insights from highly siderophile elements and Os isotopes. Geochim.
1435 Cosmochim. Acta 74, 661–683. doi:10.1016/j.gca.2009.10.007.
1436 Walker R. J. 2009. Highly siderophile elements in the Earth, Moon and Mars: update and
1437 implications for planetary accretion and differentiation. Chem. Erde-Geochem. 69, 101–
1438 125.
1439 Wang, K. L., O'Reilly, S. Y., Griffin, W. L., Pearson, N. J., Zhang, M. 2009. Sulfides in
1440 mantle peridotites from Penghu Islands, Taiwan; melt percolation, PGE fractionation,
1441 and the lithospheric evolution of the South China block. Geochim. Cosmochim. Acta 73,
1442 4531–4557. doi:10.1016/j.gca.2009.04.030.

1443 Wang, Z., Becker, H. 2013. Ratios of S, Se and Te in the silicate Earth require a volatile-rich
1444 late veneer. Nature 499, 328–331. doi:10.1038/nature12285.
1445 Wang, Z., Becker, H., Gawronski, T. 2013. Partial re-equilibration of highly siderophile
1446 elements and the chalcogens in the mantle: A case study on the Baldissero and
1447 Balmuccia peridotite massifs (Ivrea Zone, Italian Alps). Geochim. Cosmochim. Acta
1448 108, 21-44. http://dx.doi.org/10.1016/j.gca.2013.01.021.
1449 Wang, Z., Becker., H. 2015a. Fractionation of highly siderophile and chalcogen elements
1450 during magma transport in the mantle: Constraints from pyroxenites of the Balmuccia
1451 peridotite massif. Earth Planet. Sci. Lett. 159, 244-263.
1452 Wang, Z., Becker, H. 2015b. Comment on "A non-primitive origin of near-chondritic S–Se–
1453 Te ratios in mantle peridotites: Implications for the Earth's late accretionary history" by
1454 König S. et al. [Earth Planet. Sci. Lett. 385 (2014) 110–121]. Earth Planet. Sci. Lett. 417,
1455 164-166. http://dx.doi.org/10.1016/j.epsl.2013.10.036.
1456 Warren, J. M., Shirey, S. B. 2012. Lead and osmium isotopic constraints on the oceanic
1457 mantle from single abyssal peridotite sulfides. Earth. Planet. Sci. Lett. 359-360, 279-293.
1458 Wells, P. R. A. (1977). Pyroxene in simple and complex systems. Contrib. Mineral. Petrol.
1459 62, 62-129.
1460 Wendlandt, R. F. 1982. Sulfide saturation of basalt and andesite melts at high pressures and
1461 temperatures. Amer. Mineral. 67, 877– 885.
1462 Wilshire, H. G., Meyer, C. E., Nakata, J. K., Calk, L. C., Shervais, L. W., Nielson, J. W.,
1463 Schwarzman, E. G. 1988. Mafic and Ultramafic Xenoliths from Volcanic Rocks of the
1464 Western United States. US Geological Survey Professional Paper 1443. pp 1-179.
1465 Wombacher, F., Ziegler, A., Becker, H. 2009. Selenium and tellurium abundances in mafic
1466 and ultramafic rock reference samples by ID-ICP-MS. Geochim. Cosmochim. Acta
1467 73(13), A1450.

Wood, B. J., Blundy, J. D. 2001. The effect of cation charge on crystal-melt partitioning of trace elements. Earth Planet. Sci. Lett. 188, 59-71.

Yaxley, G. M., Crawford, A. J., Green, D. H. 1991. Evidence for carbonatite metasomatism in spinel lherzolite xenoliths. Earth Planet. Sci. Lett. 107, 305-317.

Yu, M. Q., Liu, G. Q., Jin Q. 1983. Determination of trace arsenic, antimony, selenium and tellurium in various oxidation states in water by hydride generation and atomic-absorption spectrophotometry after enrichment and separation with thiol cotton. Talanta 30(4), 265–270.

Zhang, H. F., Ying, J. F., Tang, Y. J., Zhang J. 2004. Transformation of lithospheric mantle from old refractory to young fertile through peridotite‑melt interaction. Geochim. Cosmochim. Acta 68. A711.

Figure captions

Figure 1. Mineral modal abundances preserved in Kilbourne Hole xenoliths from this study. The calculated mineral modal abundances of most samples are consistent with varying degrees of melt depletion. For comparison, the effects upon modal mineralogy of experimental 1-20% batch melting (large dashes) of Baker and Stolper (1994) and repeated extraction of small batch melts (small dashes; Robinson et al., 1998) are illustrated. Light gray symbols (group 2) are xenoliths with bulk-rock $(La/Yb)_N$ >1 (where $(La/Yb)_N$ is the

ratio of La/Yb normalised to the composition of primitive mantle; McDonough and Sun, 1995) dark gray symbols (group 1) are xenoliths with $(La/Yb)_N$ <1. Numbers in symbols refer to KH96 xenoliths (italics) or KH03 xenoliths (non-italicized). Crossed field = non-cratonic peridotite xenoliths; striped field = cratonic peridotites (Pearson et al., 2004). Figure modified after Harvey et al. (2012).

Figure 2. Relationship between melt depletion, silicate and sulfide metasomatism in the Kilbourne Hole peridotite xenoliths from this study. (a) Al_2O_3 wt. % versus $(La/Yb)_N$, (striped rectangle = Primitive mantle (PM); O'Neill, 1991; McDonough and Sun 1995; Becker et al., 2006). Symbols as in Figure 1. Data from Harvey et al. (2012). Grey field represents field of compositions possible from 1-20 % non-modal fractional melting alone. (b) Osmium isotope ratios as a function of melt depletion. Both sample suites demonstrate strong co-variations with Al_2O_3. The group 2 samples project to values in excess of PM, whereas the group 1 samples project to approximately the value of PM. Modified after Figure 2a of Harvey et al. (2011). (c) Unlike the $^{187}Os/^{188}Os$ ratio, there is significantly more scatter in Re/Os for a given degree of melt depletion in group 2 samples. Data from Harvey et al., (2011, 2012). Error bars show 2σ reproducibility. Where no error bars are shown the 2σ uncertainty is smaller than the symbol used.

Figure 3. Back-scattered electron image of sulfide in KH03-20.

Figure 4. S-Se-Te versus Al_2O_3. (a) No strong relationship is observed between S and Al_2O_3, despite both of these elements being considered suitable as indices of melt depletion (e.g. Burnham et al., 1998; Reisberg and Lorand, 1995, respectively). While most of the peridotites define a broad positive co-variation, some samples in both subsets extend to

1518 higher S abundances for a given Al_2O_3. (b) A similar relationship to that observed in (a) can
1519 be seen with regard to Se, although correlation coefficients are marginally stronger between
1520 Se and Al_2O_3. (c) Correlation coefficients between Te and Al_2O_3 are marginal, suggesting
1521 little or no relationship between melt depletion alone and Te abundance in these xenoliths.
1522 Symbols as in Figure 2 with small black circles from Morgan (1996). Small white circles are
1523 literature data from Lorand et al. (2010, 2012), Alard et al. (2011), König et al. (2012, 2014),
1524 Wang et al. (2013), with additional Al_2O_3 data from Le Roux et al. (2007).
1525
1526 **Figure 5**. S-Se-Te abundances. Symbols as in Figure 1. Grey field = CI chondrite (Palme and
1527 Jones, 2003). (a) Both sample subsets demonstrate a strong positive co-variation in S and Se
1528 abundances. (b) The co-variation between Te and S is less strong, notably in group 1 samples.
1529 (c) This is also reflected in the Te versus Se positive co-variation which is marked in group 2
1530 samples, but absent in group 1 samples. Small white circles are literature data from Lorand et
1531 al. (2010, 2012), Alard et al. (2011), König et al. (2012, 2014), Wang et al. (2013). Primitive
1532 mantle (PM; striped rectangle) defined by O'Neill, 1991, McDonough and Sun (1995) and
1533 Becker et al. (2006). Small black circles are Kilbourne Hole peridotites from Morgan (1986).
1534
1535 **Figure 6.** Platinum group element abundances, normalized to the composition of Primitive
1536 Mantle (Becker et al., 2006). (a) Group 1 samples (b) Group 2 samples. Rhenium abundances
1537 vary by up to 15% (see analytical methods sections) but error bars have not been added for
1538 clarity.
1539
1540 **Figure 7.** Co-variation of HSE in group 1 and 2 peridotite xenoliths. Strong co-variations
1541 exist in the group 1 peridotites between (a) Ir and Os, (b) Pd and Pt, (c) Re and Pt and (d) Re
1542 and Ir, i.e., all of the HSE behave in a similar manner which is not consistent with melt

depletion, but more likely removal of sulfide in a S-undersaturated melt. Strong co-variations are observed within the group 2 peridotites between (a) Ir and Os (IPGE) and (b) Pt and Pd (PPGE), but no strong positive covariation between IPGE, PPGE and / or Re, which is consistent with fractionation resulting from melt depletion.

Figure 8. Pd and Re co-variation with S, Se and Te. Strong positive correlations are apparent between Pd and S (a) and Pd and Se (b) for both subsets of peridotites. The predicted residual composition after 0-20 % non-modal fractional melt depletion is shown inset. The model assumes a primitive mantle (PM) starting composition ([Pd] = 7.7 ng g^{-1}, Becker et al (2006); [S] = 250 ± 50 µg g^{-1}, (O'Neill, 1991; Lorand 1990, Palme and O'Neill, 2003); [Se] = 79 ng g^{-1}, (Palme and O'Neill, 2003; König et al, 2014). Modelled curves for $D_{Pd}^{sulfide/melt}$) = 10^5 and 10^3 from Wang et al (2013), Se depletion from Wang et al (2013), which assumes a $D^{sulfide/melt}$ of 1770. Model assumes sulfur concentration at sulfur saturation of 10^3 µg g^{-1} S throughout. (c) Pd and Te in group 2 peridotites have much stronger correlations than group 1 samples. (PM [Te] = 12 ng g^{-1} (König et al, 2014)). D^{sulf} from Handler and Bennett (1999). A similar strong positive correlation between Re and S (d) is also observed (PM [Re] = 0.32 ppb, (Palme and O'Neill, 2003). Modelled depletion of Re assumes a similar bulk partition coefficient to that of Yb during partial melting (Blundy and Wood, 2003). This relationship breaks down for Re and Se (e) in group 2 samples, yet remains strong in group 1 peridotites. Like Pd vs. Te, there is a very strong positive correlation between Re and Te (f) in group 2, with no apparent correlation in group 1 peridotites. Symbols as per Figure 1. Where error bars are not shown 2σ uncertainty is smaller than symbol size.

Figure 9. Relationship between degree of silicate metasomatism, i.e., $(La/Yb)_N$, and (a) sulfur (b) selenium (c) tellurium (d) osmium (e) iridium (f) platinum (g) palladium and (h)

rhenium. Neither of the subsets of peridotites show any particularly strong correlations between $(La/Yb)_N$ and S, Se, Te or PPGE, although group 2 peridotites are more strongly (negatively) correlated with the degree of silicate metasomatism than group 1 peridotites. The only elements that deviate from this pattern are the IPGE, which have slight (R^2 = 0.13) to moderate (R^2 = 0.53) positive co-variations with degree of silicate metasomatism. Primitive mantle compositions from Lorand (1990); O'Neill (1991); Palme and O'Neill (2003); Becker et al. (2006); König et al. (2014). Symbols as in Figure 1. Where error bars are not shown 2σ uncertainty is smaller than symbol size.

Figure 10. Cartoon depicting the likely sequence of events affecting the HSE abundances of (a) group 1 and (b) group 2 peridotites. Group 1 peridotites experienced (i) varying degrees (<20 %) of melt depletion followed by (ii) dilution of all of the HSE concentrations through the removal of sulfide by a S-undersaturated melt. After exposure at the surface of the Earth as a peridotite xenolith, supergene weathering partially oxidizes sulfide and Os is removed in its volatile OsO_4 form. Group 2 peridotites also experienced up to 20% partial melting (i) followed by (ii) the addition of metasomatic sulfide which drove HSE patterns back towards a PUM-like composition (and in the case of KH03-3 and KH03-24, cf. Figure 8) beyond PUM abundances for the PPGE. Finally, like the group 1 peridotites, supergene weathering oxidized sulfide and removed Os (iii).

Figure 11. Covariation of HSE abundance and S abundance. (a) Iridium abundances tend to be invariant with all but the lowest sulfur abundances. Ir, Pd (b) and Pt (c) scatter crudely around model calculations for bulk-rock HSE abundances with varying degrees of melt depletion. Model parameters from Handler and Bennett (1999).

Figure 12. Se/Te variability as a function of Te abundance. Despite S abundance being considered a useful index of melt depletion (e.g. Burnham et al., 1998) and recent estimates for partition coefficients for $Se^{mss/sulfide\ melts}$, $Te^{mss/sulfide\ melts}$ (Helmy et al., 2010) and $Se^{solid/melt}$ and $Te^{solid/melt}$ (van Acken et al., 2010a), no systematic behavior with increasing degree of melt depletion is observed, except perhaps an increase in Se/Te at the lowest Te abundances. See also Figure 3 for poor degrees of correlation between S-Se-Te and bulk-rock Al_2O_3 wt. %. (i) batch melt depletion curve, (ii) incremental melt depletion curve, (iii) "forced" melt depletion curve parameters from König et al. (2014) - see main text for details.

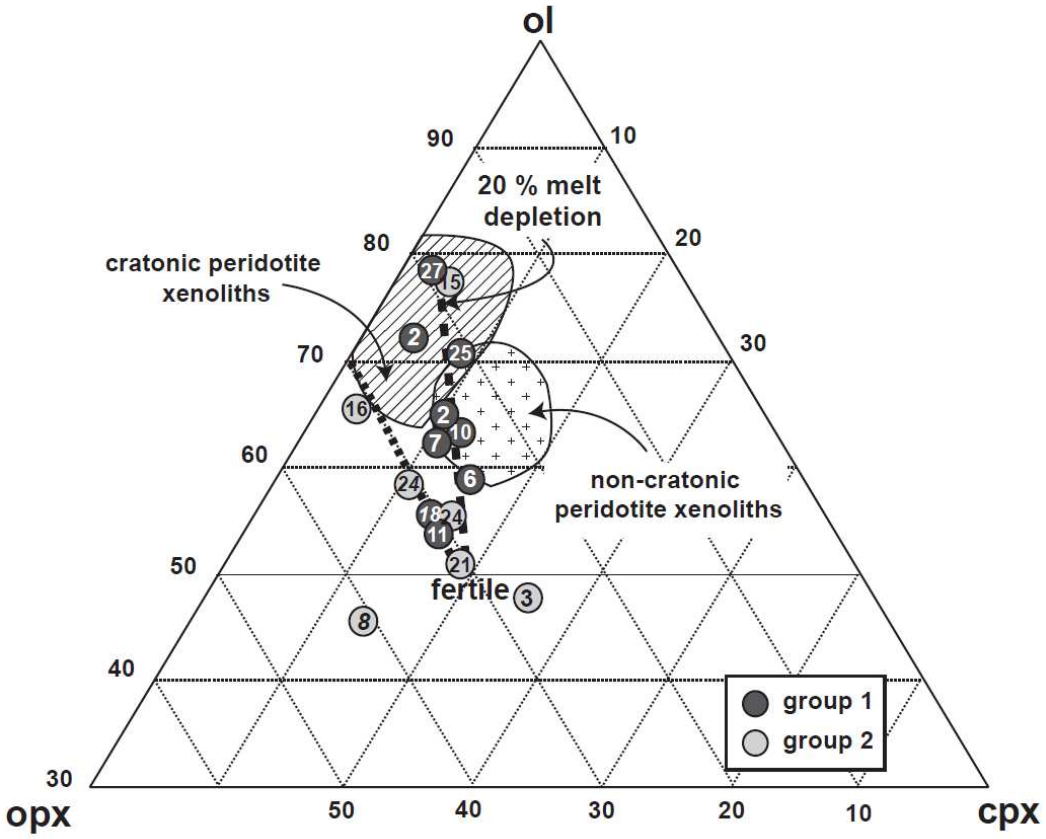
ol
90
10
20 % melt
depletion
80
20
cratonic peridotite
xenoliths
27
5
2
70
25
30
16
2
7
10
60
6
24
non-cratonic
peridotite xenoliths
18
4
11
50
21
fertile
3
8
40
group 1
group 2
30
opx
50
40
30
20
10
cpx

Figure 1

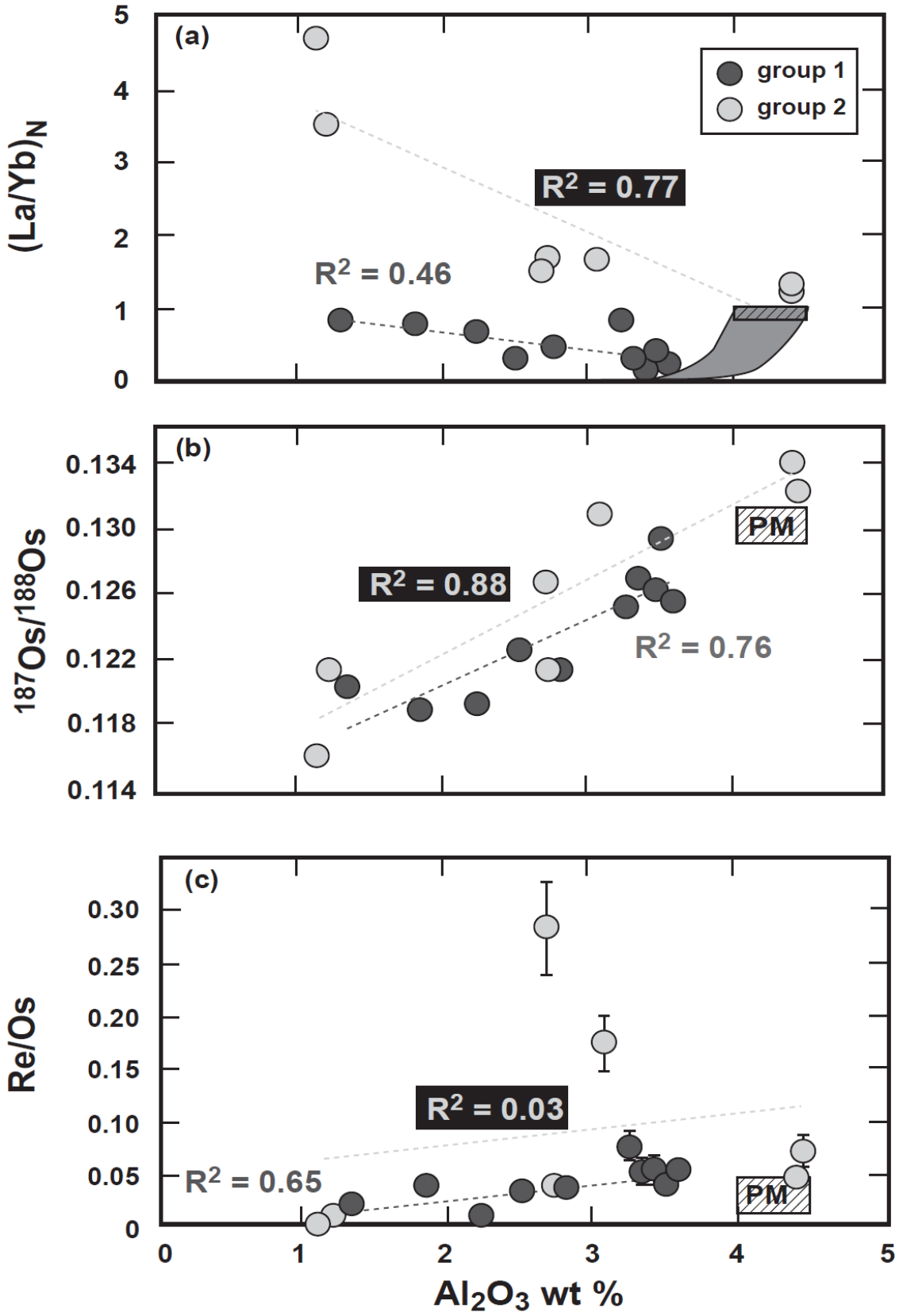

1631

1632 Figure 2

1633

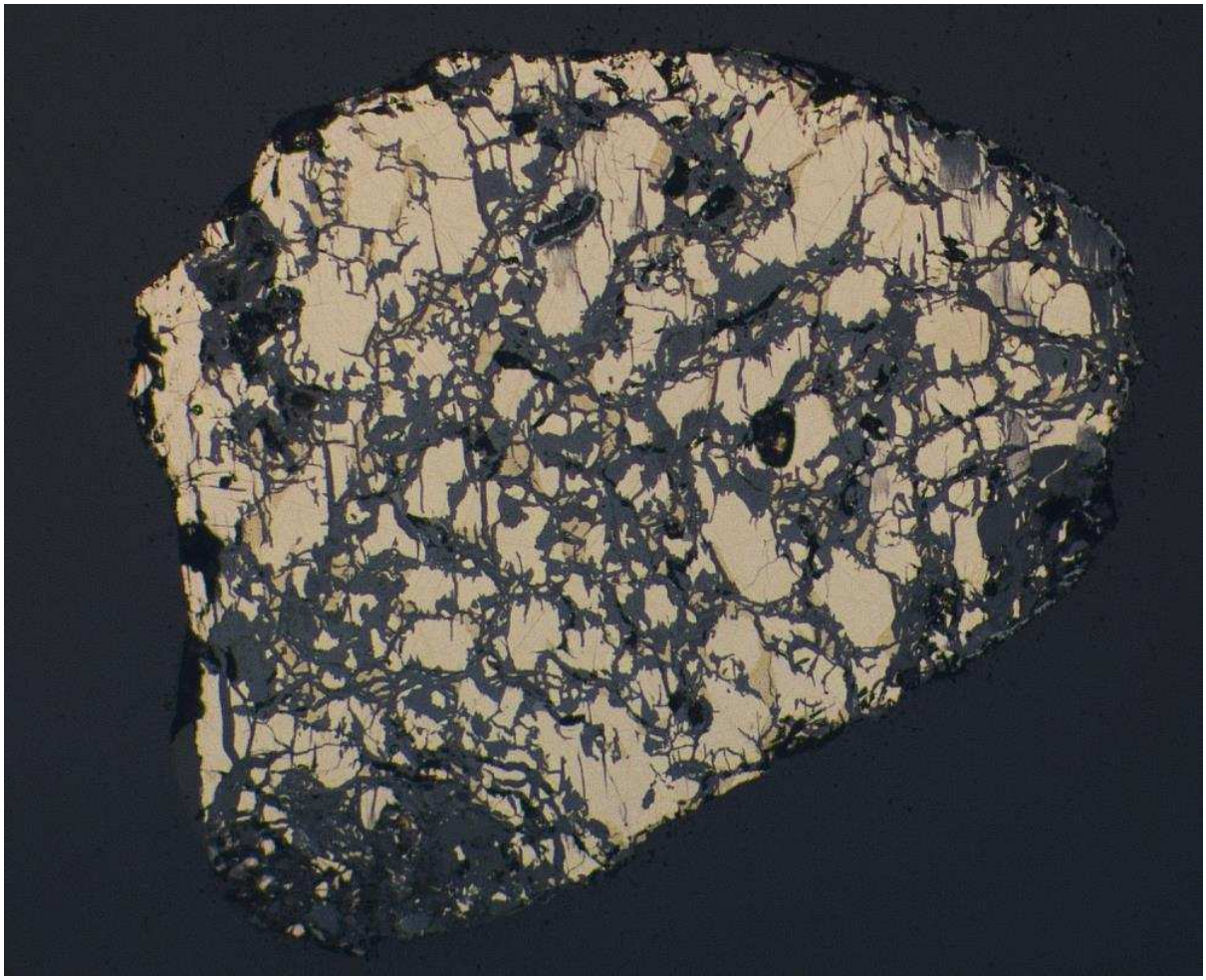

Figure 3

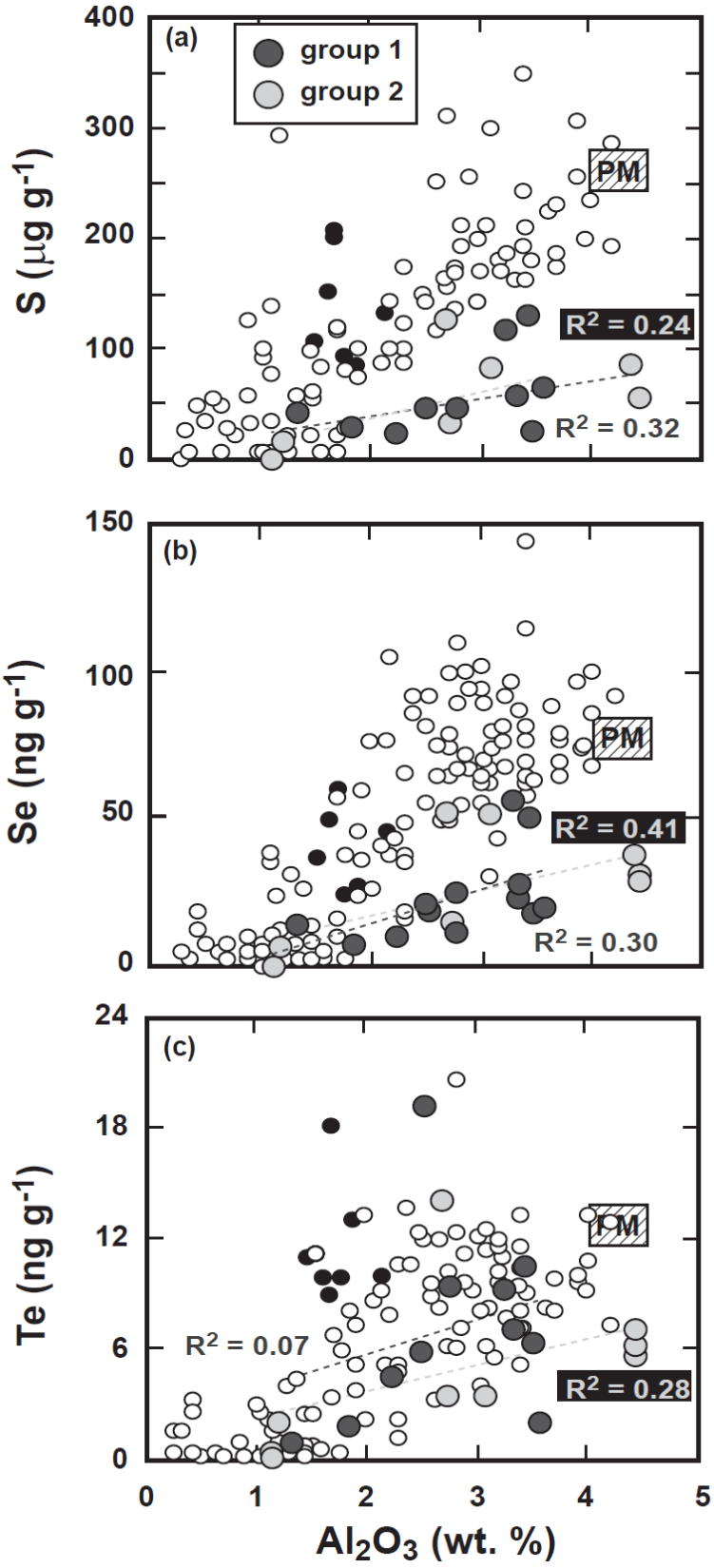

1647

1648 Figure 4

1649

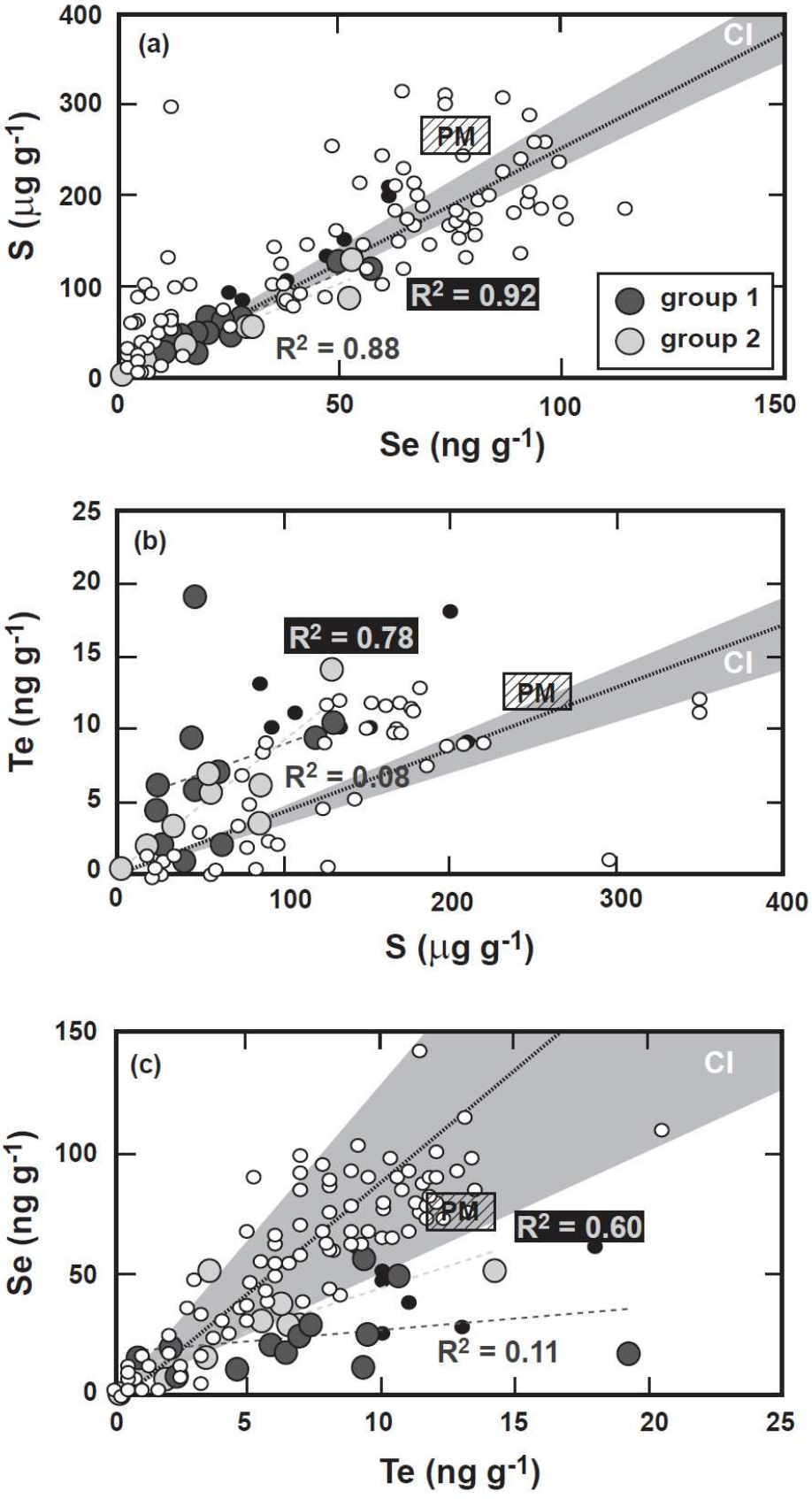

1650

1651 Figure 5

1652

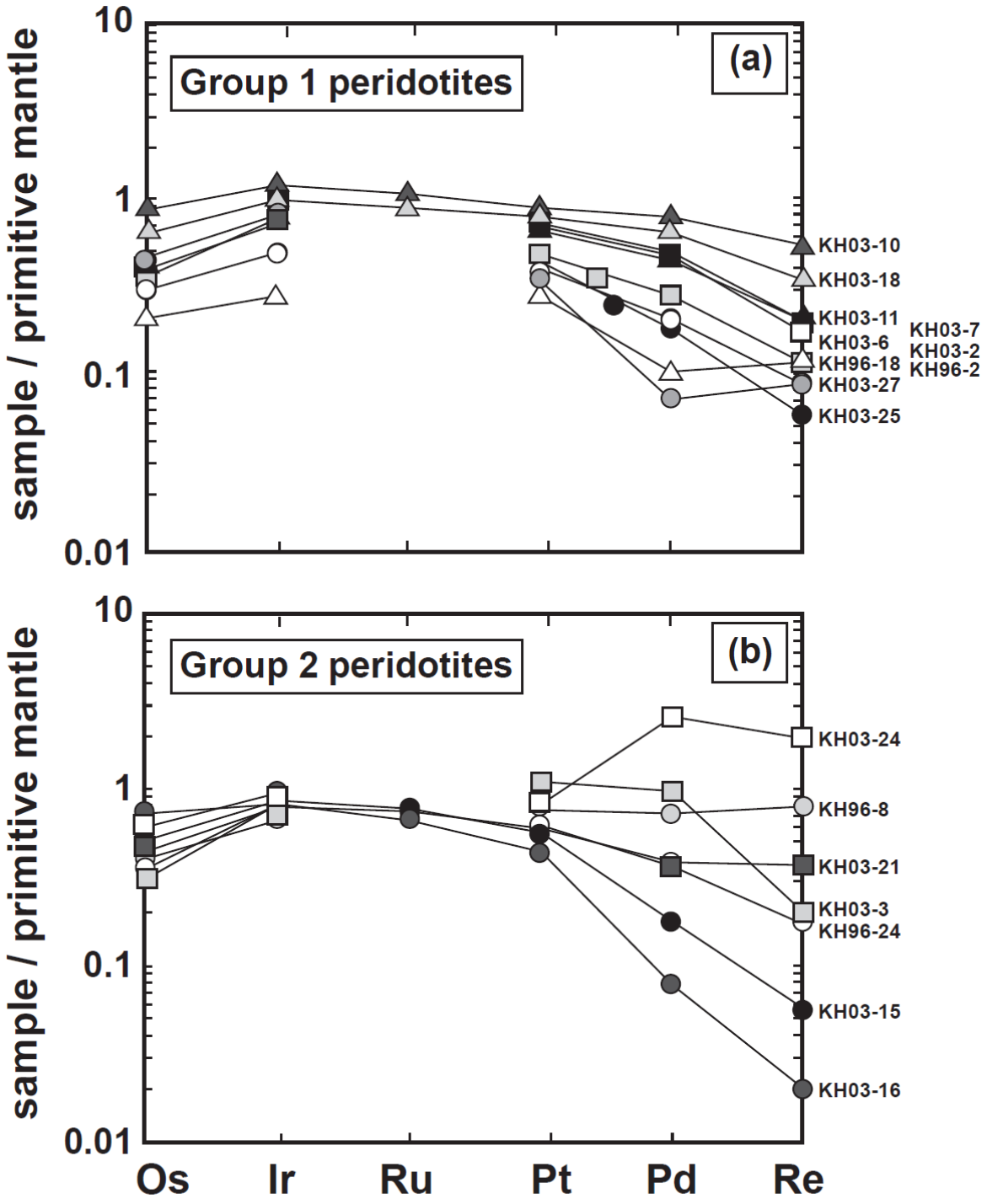

1653

1654 Figure 6

1655

1656

1657

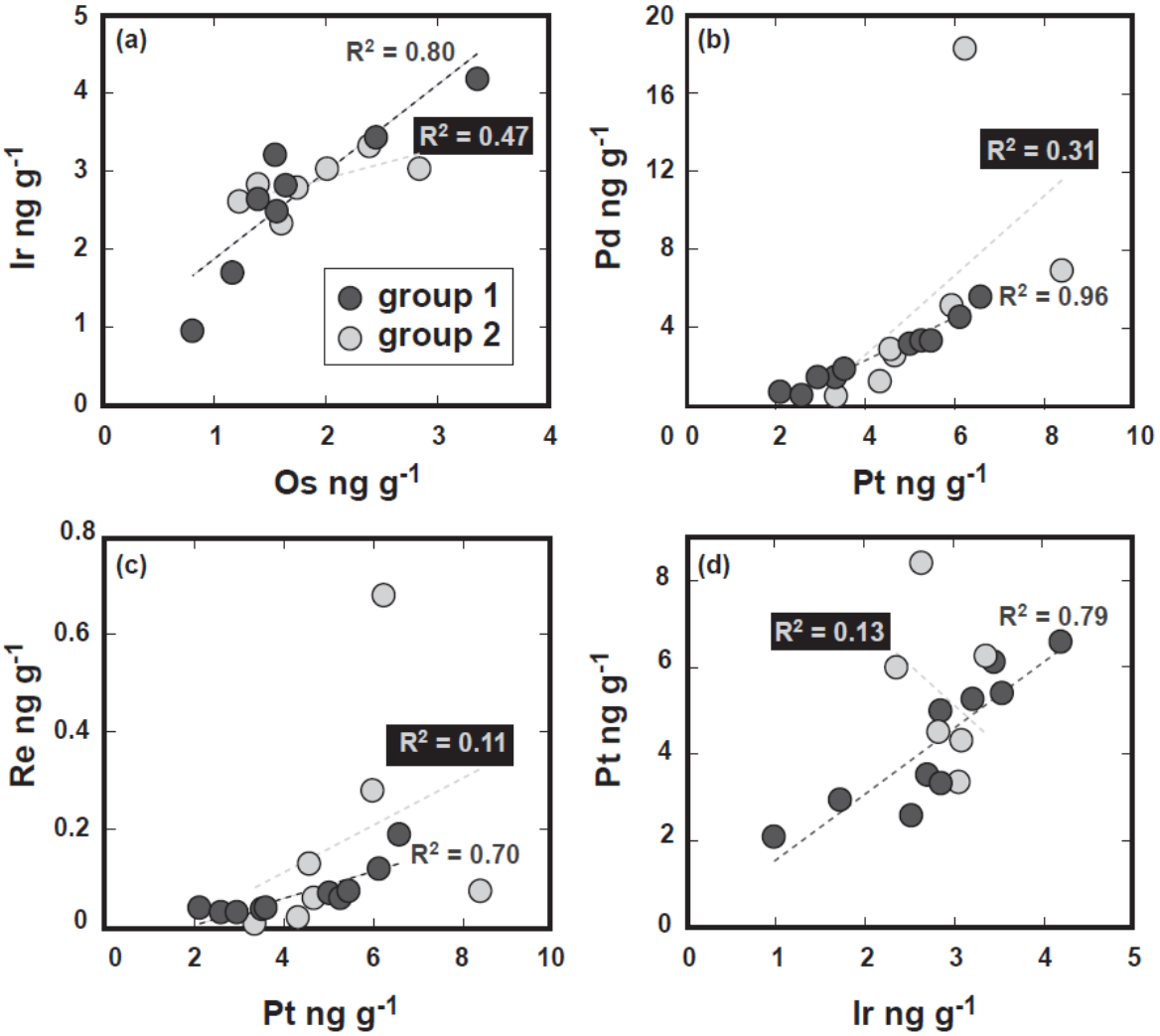
(a)
R² = 0.80
R² = 0.47
group 1
group 2
Ir ng g-1
Os ng g-1
(b)
R² = 0.31
R² = 0.96
Pd ng g-1
Pt ng g-1
(c)
R² = 0.11
R² = 0.70
Re ng g-1
Pt ng g-1
(d)
R² = 0.13
R² = 0.79
Pt ng g-1
Ir ng g-1

Figure 7

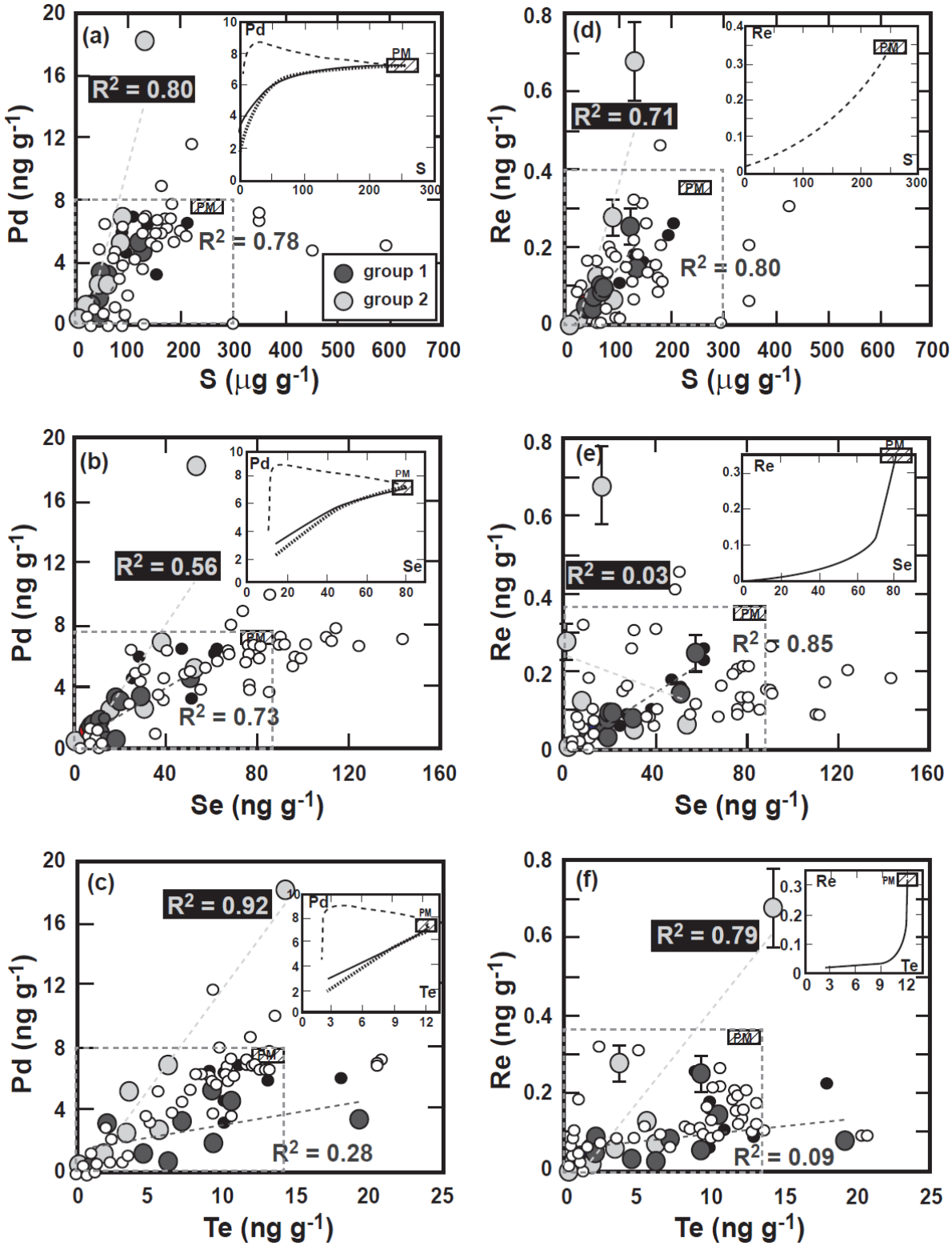

1669

1670 Figure 8

1671

1672

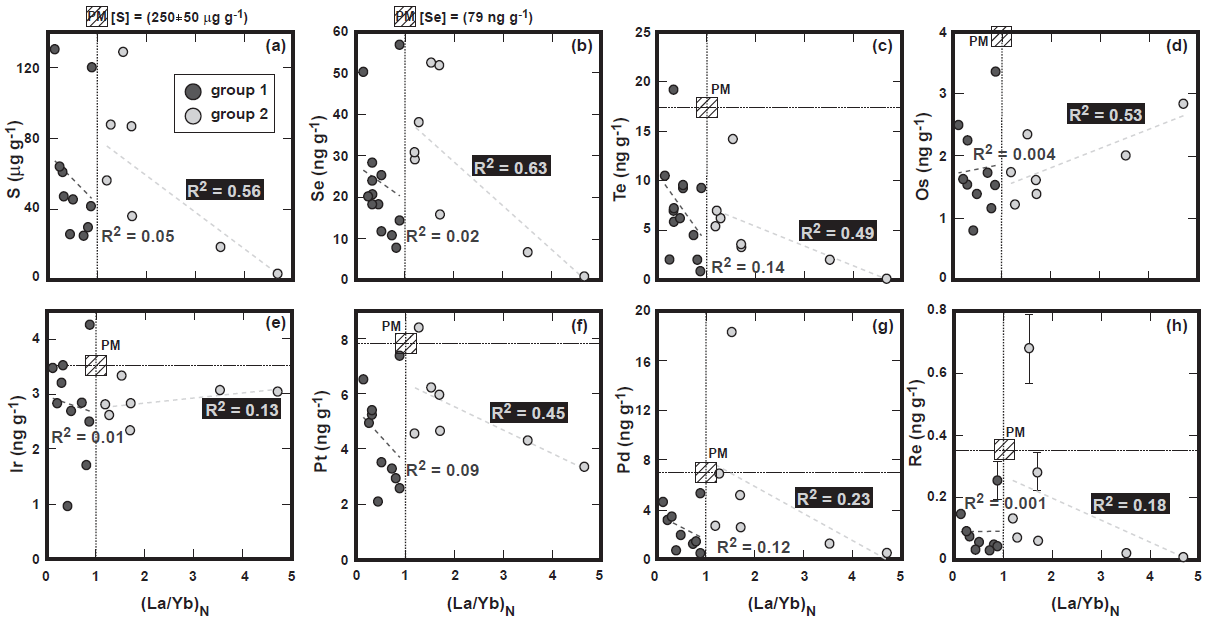
PM [S] = (250±50 µg g-1)
PM [Se] = (79 ng g-1)
(a)
(b)
(c)
(d)
(e)
(f)
(g)
(h)
group 1
group 2
S (µg g-1)
Se (ng g-1)
Te (ng g-1)
Os (ng g-1)
Ir (ng g-1)
Pt (ng g-1)
Pd (ng g-1)
Re (ng g-1)
PM
R2 = 0.56
R2 = 0.05
R2 = 0.63
R2 = 0.02
R2 = 0.49
R2 = 0.14
R2 = 0.53
R2 = 0.004
R2 = 0.13
R2 = 0.01
R2 = 0.45
R2 = 0.09
R2 = 0.23
R2 = 0.12
R2 = 0.001
R2 = 0.18
(La/Yb)N

Figure 9

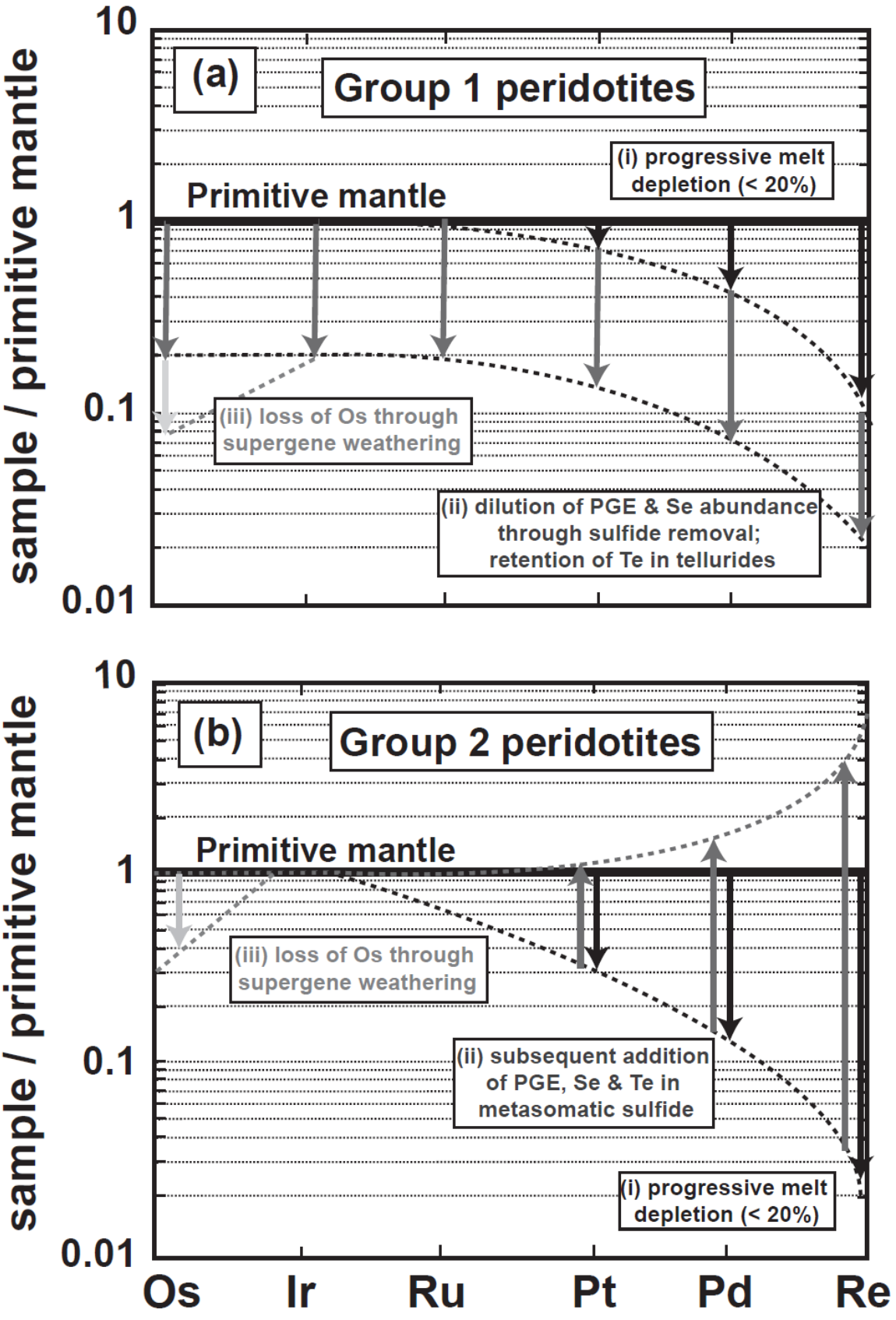

1690

1691 Figure 10

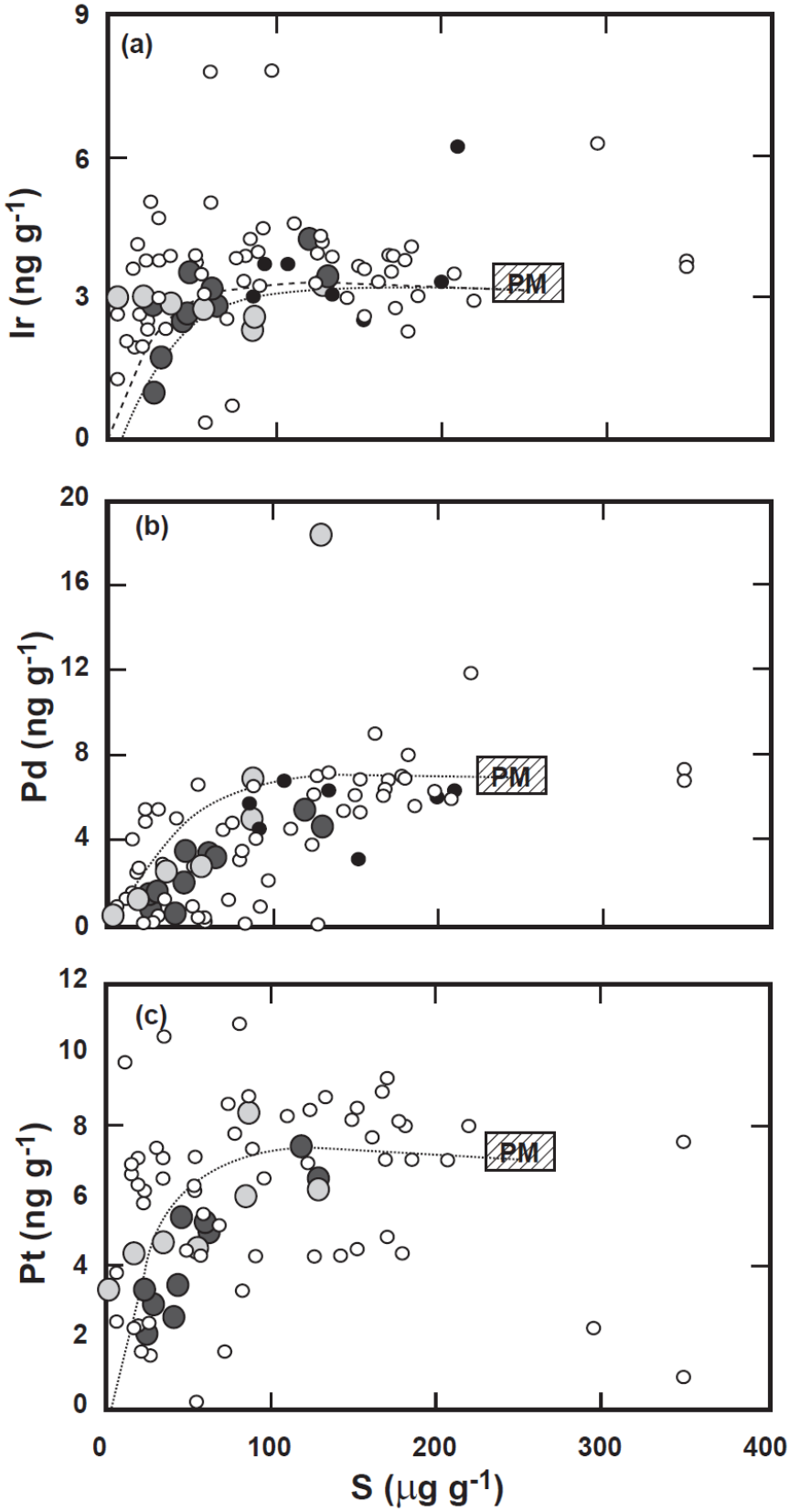

1692

1693 Figure 11

1694

	S	Se	Te	Se/Te	Ir	Pt	Pd	Re

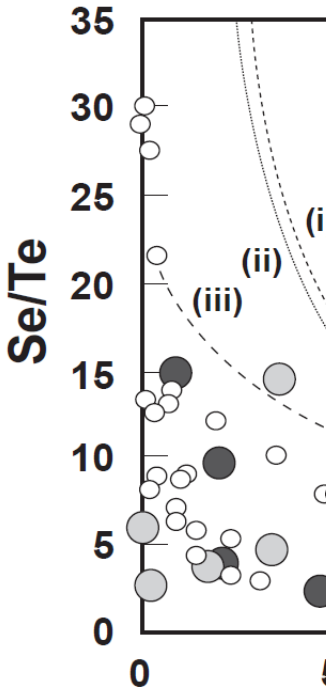

1695

1696 Figure 12

1697

1698

1699

1700

1701

1702

1703

1704

1705

1706

1707

1708

1709

UBN-1	[a]	132	10.2	12.9	[a]	[a]	[a]	[a]
UBN-1	[a]	[a]	[a]	[a]	2.93	7.48	5.80	0.18
UBN-1	[a]	[a]	[a]	[a]	2.94	7.13	5.53	0.19
UBN-1	[a]	[a]	[a]	[a]	2.92	7.41	5.63	0.17
UBN-1 mean	-	-	-	-	2.93	7.34	5.65	0.18
UBN-1 (2σ)	-	-	-	-	0.02	0.37	0.27	0.03
PCC-1	17	[a]	[a]	[a]	[a]	[a]	[a]	[a]
Blk	3	bdl	bdl	-	0.001	0.008	0.026	0.006
Blk	[a]	bdl	bdl	-	0.004	0.017	0.024	0.005
Blk	[a]	bdl	bdl	-	0.001	0.011	0.017	0.007
Blk mean	3	-	-	-	0.002	0.012	0.022	0.006
Blk (2σ)	-	-	-	-	0.001	0.004	0.005	0.001

Table 1. Analysis of reference materials and total procedural blank analyses. Sulfur abundances expressed in µg g^{-1}, all others in ng g^{-1}. [a]denotes not analysed. bdl denotes below detection limits. Abundances of Os and Ru, where available, can be found in Harvey et al. (2011)

Table 2. Abundances of S, Se, Te, platinum group elements and Re. [a]Sulphur abundances expressed in μg g^{-1}, all other abundances in ng g^{-1}. [b]Osmium concentrations derived from powder splits prepared for Harvey et al. (2011) [c]blank-corrected Re abundance, with % of blank correction. [d]duplicate measurement. [e]not determined. Group 1 peridotites are distinguished by $(La/Yb)_N$ <1 compared to group 2 peridotites which have $(La/Yb)_N$ >1. Al_2O_3 wt. % from Harvey et al. (2011).

Sample	Al_2O_3 wt %	S[a]	Se	Te	Os[b]	Ir	Ru	Pt	Pd	Re[c]	blk %
Group 1 peridotites											
KHO3-2	2.76	46	11.8	9.3	1.39	2.69	[e]	3.52	1.97	0.03	15
KHO3-2[d]		[e]	25.3	9.4	[e]	[e]	[e]	[e]	[e]	[e]	[e]
KHO3-6	3.32	61	28.3	7.2	1.54	3.20	[e]	5.26	3.35	0.05	10
KHO3-6[d]		[e]	24.0	7.0	[e]	[e]	[e]	[e]	[e]	[e]	[e]
KHO3-7	2.51	47	18.6	19.2	[e]	3.53	[e]	5.40	3.45	0.06	9
KHO3-7[d]		[e]	20.8	5.9	[e]	[e]	[e]	[e]	[e]	[e]	[e]
KHO3-10	3.23	120	56.9	9.3	3.36	4.19	7.47	6.58	5.58	0.18	3
KHO3-11	3.55	64	20.3	2.1	1.63	2.83	[e]	4.98	3.18	0.06	9
KHO3-18	3.41	130	50.1	10.5	2.45	3.44	6.21	6.12	4.55	0.11	5
KHO3-25	2.22	25	10.9	4.5	1.73	2.83	[e]	3.32	1.27	0.01	30
KHO3-27	1.32	42	14.4	1.0	1.54	2.51	[e]	2.58	0.50	0.02	20
KH96-2	1.83	30	7.86	2.1	1.16	1.71	[e]	2.94	1.45	0.02	20
KH96-18	3.46	26	18.3	6.2	0.80	0.97	[e]	2.10	0.72	0.04	15
Group 2 peridotites											
KHO3-3	4.37	88	38.2	6.2	1.22	2.62	[e]	8.40	6.93	0.06	9
KHO3-15	1.20	19	6.9	1.9	2.01	3.07	5.43	4.31	1.26	0.01	30
KHO3-16	1.13	<3	1.1	0.4	2.84	3.04	4.77	3.35	0.55	0.001	86
KHO3-16[d]		[e]	0.9	0.2	[e]	[e]	[e]	[e]	[e]	[e]	[e]
KHO3-21	4.41	56	30.7	5.5	1.74	2.81	5.25	4.56	2.74	0.12	5
KHO3-21[d]		[e]	29.2	6.6	[e]	[e]	[e]	[e]	[e]	[e]	[e]
KHO3-21[d]		[e]	29.5	6.9	[e]	[e]	[e]	[e]	[e]	[e]	[e]
KHO3-24	2.72	36	15.9	3.4	2.39	3.33	[e]	6.23	18.30	0.67	1
KH96-8	3.06	87	51.9	3.6	1.60	2.34	[e]	5.97	5.18	0.27	2
KH96-24	2.67	129	52.6	14.2	1.39	2.84	5.14	4.66	2.59	0.05	10

Table S1. Lithology, texture, mineral modal abundance and equilibration temperature for the Kilbourne Hole peridotite xenoliths of this study. Data from Harvey et al. (2012). All samples recovered from within a 200 metre radius of N 031.57.595 W 106.58.148. [a]Not determined. [b]Lithology: L = lherzolite, H = harzburgite. [c]Texture based upon criteria of Mercier & Nicolas (1975): i, protogranular; ii, transitional between protogranular aa porphyroclastic. [d]Modal abundance calculated using a total inversion method (Tarantola & Valette, 1982), which utilizes bulk-rock and mineral major element abundances. Ol = olivine; Opx = orthopyroxene; Cpx = clinopyroxene; Spl = spinel. Uncertainties on modal abundance are ± 2·9% for olivine, ± 3·6% for orthopyroxene, ± 1·7% for clinopyroxene, ± 0·9% forspinel. [e]Calculated using the two-pyroxene geothermometer of Wells (1977). [f]Calculated using the two-pyroxene geothermometer of Brey & Kohler (1990).

			Modal abundance[d]				Equilibration temperature °C			
Sample	Lithology[b]	Texture[c]	Ol	Opx	Cpx	Spl	Wells[e]	±	B and K[f]	±
KH03-2	L	i	63.5	23.6	10.9	2.1	983	13	1020	12
KH03-3	L	i	46.8	26.2	23.9	3	978	13	1014	13
KH03-6	L	i	59.1	25	14.2	1.6	971	10	1002	10
KH03-7	L	i	62.6	25.9	10.7	0.9	1003	8	1047	6
KH03-10	L	i	62.4	23.9	12	1.8	1039	7	1085	6
KH03-11	L	i	53.2	29.7	15.7	1.4	970	10	1014	10
KH03-15	H	i	76.9	18	3.9	1.2	1126	7	1165	5
KH03-16	H	i	64.9	30.7	2.6	1.8	1123	2	1152	1
KH03-18	[a]	[a]	[a]	[a]	[a]	[a]	[a]	[a]	[a]	[a]
KH03-21	L	ii	50.4	29.6	17.5	2.5	958	6	989	17
KH03-24	L	i	56.4	27.8	13.2	2.6	989	8	1021	7
KH03-25	L	i	70.3	20.3	8.1	1.4	1009	13	1058	17
KH03-27	H	i	79.1	18.9	2.2	0	965	8	1000	7
KH96-2	L	i	71.6	22.4	5.2	0.8	1006	8	1045	15
KH96-8	L	i	45.1	39.9	12.9	2	1143	5	1181	4
KH96-18	L	i	54.6	28.9	14.6	1.9	986	5	1025	9
KH96-24	L	i	57.6	30.9	10.1	1.5	927	6	940	11

Table S2. Bulk-rock Al_2O_3, $(La/Yb)_N$, Re and Os elemental abundance and Re-Os isotope systematics of the 17 peridotite xenoliths from this study. Al_2O_3 (expressed in wt. %) and $(La/Yb)_N$ from Harvey et al. (2012), where $(La/Yb)_N$ is La/Yb normalised to the composition of primitive mantle (McDonough and Sun, 1995), Re-Os measurements from Harvey et al. (2011). Complete major and trace element abundances can be found in Harvey et al. (2012). [Re] and [Os] expressed in ng g^{-1}. Errors shown as 2σ mean. T_{RD} = (minimum) time of rhenium depletion calculated using ($T_{RD} = 1/\lambda \times \ln \{[(^{187}Os/^{188}Os_{chon} / ^{187}Os/^{188}Os_{sample}) / ^{187}Re/^{188}Os_{chon}] + 1\}$ (Shirey and Walker, 1998) which assumes a mean present-day chondritic value $^{187}Os/^{188}Os = 0.127$ (Luck & Allègre, 1983; Walker & Morgan, 1989) and also assumes that $^{187}Re/^{188}Os_{sample} = 0$. [a] not determined. [b] T_{RD} produces no useful geochronological information. [c] Carius tube digestion. [d] high pressure asher digestion for PGE concentration measurement. [e] duplicate measurement.

Sample	$(La/Yb)_N$	[Os]	[Re]	$^{187}Os/^{188}Os$	2 s.e.	$^{187}Re/^{188}Os$	T_{RD}
KH03-2[c]	0.51	1.39	0.04	0.1213	0.0001	0.124	0.85
KH03-3[c]	1.27	1.22	0.07	0.134	0.0001	0.27	[b]
KH03-6[c]	0.31	1.54	0.06	0.1267	0.0002	0.183	0.05
KH03-6[ce]	[a]	1.6	0.08	0.1272	0.0003	0.243	[b]
KH03-6[ce]	[a]	1.48	0.06	0.1269	0.0001	0.183	0.02
KH03-6[ce]	[a]	1.52	0.06	0.127	0.0002	0.173	0
KH03-7[c]	0.32	2.25	0.07	0.1226	0.0001	0.138	0.65
KH03-10[c]	0.88	3.36	0.19	0.1252	0.0001	0.261	0.27
KH03-10[de]	[a]	3.36	0.19	[a]	[a]	[a]	[a]
KH03-10[de]	[a]	3.23	0.23	[a]	[a]	[a]	[a]
KH03-11[c]	0.23	1.63	0.07	0.1257	0.0002	0.2	0.19
KH03-15[c]	3.51	2.01	0.02	0.1213	0.0002	0.044	0.84
KH03-15[de]	[a]	2.01	0.02	[a]	[a]	[a]	[a]
KH03-15[de]	[a]	2.04	0.03	[a]	[a]	[a]	[a]
KH03-16[c]	4.68	2.84	0.01	0.116	0.0003	0.009	1.62
KH03-16[de]	[a]	2.96	0.002	[a]	[a]	[a]	[a]
KH03-16[de]	[a]	3.04	0.01	[a]	[a]	[a]	[a]
KH03-18[c]	0.13	2.5	0.12	0.1263	0.0004	0.214	0.11
KH03-18[de]	[a]	2.4	0.16	[a]	[a]	[a]	[a]
KH03-18[de]	[a]	2.5	0.12	[a]	[a]	[a]	[a]
KH03-21[c]	1.19	1.72	0.13	0.1325	0.0001	0.306	[b]
KH03-21[ce]	[a]	1.71	0.07	0.1324	0.0001	0.185	[b]
KH03-21[ce]	[a]	1.79	0.06	0.1322	0.0003	0.151	[b]

KH03-21[de]	a	1.72	0.13	a	a	a	a
KH03-21[de]	a	1.71	0.07	a	a	a	a
KH03-21[de]	a	1.79	0.06	a	a	a	a
KH03-21[de]	a	1.73	0.08	a	a	a	a
KH03-24[c]	1.71	1.39	0.06	0.1233	0.0001	0.148	0.54
KH03-24[ce]	a	1.79	0.04	0.1192	0.0002	0.077	1.16
KH03-24[de]	a	1.39	0.06	a	a	a	a
KH03-24[de]	a	1.39	0.05	a	a	a	a
KH03-25[c]	0.72	1.73	0.02	0.1194	0.0002	0.052	1.13
KH03-27[c]	0.87	1.54	0.03	0.1203	0.0033	0.088	0.99
KH96-2[c]	0.8	1.16	0.03	0.1189	0.0001	0.124	1.21
KH96-8[c]	1.7	1.6	0.28	0.1309	0.0001	0.832	b
KH96-18[c]	0.43	0.8	0.04	0.1294	0.0001	0.196	b
KH96-24[c]	1.53	2.39	0.68	0.1268	0.0001	1.36	0.03

Table S3. Major element abundances of sulfide grains in peridotite xenoliths from Kilbourne Hole, New Mexico, USA. Repeat analyses of an in-house pentlandite standard yields errors on major elements (S, Fe, Ni) of 2, 5 and 6 % (2 σ) respectively, with minor elements (Co, Cu) errors (2 σ) of 22% and 70% respectively (Data from Harvey et al., 2011).

Sample	Ni	Cu	S	Fe	Co	Zn	Si	Total
KH03-11_A1	16.03	0.61	36.69	45.34	0.31	0.00	0.03	99.00
KH03-11_A1	34.14	1.31	33.20	31.15	0.46	0.00	0.01	100.27
KH03-14_A10	16.02	0.78	37.48	44.28	0.31	0.00	0.00	98.87
KH03-14_A10	8.89	4.44	37.16	48.88	0.23	0.00	0.00	99.61
KH03-14_A10	1.74	20.99	34.81	40.17	0.14	0.02	0.00	97.86
KH03-14_A9	15.03	0.63	37.35	45.50	0.31	0.00	0.00	98.83
KH03-14_A8	17.71	0.44	36.37	43.70	0.28	0.00	0.00	98.50
KH03-14_A8	11.40	11.69	35.25	39.97	0.19	0.01	0.00	98.51
KH03-14_A9	1.92	21.44	35.15	39.75	0.13	0.01	0.00	98.40
KH03-14_A7	19.50	4.56	35.08	35.84	0.36	0.02	1.15	96.50
KH03-14_A7	16.13	0.66	37.49	44.63	0.30	0.00	0.00	99.21
KH03-14_A6	13.30	0.44	37.24	47.52	0.26	0.00	0.00	98.76
KH03-14_A5	17.05	0.77	37.19	44.18	0.29	0.00	0.00	99.48
KH03-14_A4	15.76	0.73	37.50	45.33	0.30	0.00	0.00	99.63
KH03-14_A3	14.78	0.37	38.08	45.09	0.30	0.00	0.01	98.63
KH03-14_A2	14.66	0.55	37.64	45.99	0.31	0.01	0.00	99.16
KH03-14_A1	15.14	0.77	37.31	45.98	0.31	0.00	0.00	99.52
KH03-15_1.1	28.76	0.68	34.71	35.01	0.30	0.00	0.00	99.47
KH03-17_A1	23.26	0.23	37.93	38.17	0.29	0.00	0.00	99.87
KH03-17_A2	25.88	0.31	37.75	35.64	0.29	0.01	0.00	99.87
KH03-21_1.1	29.39	1.72	32.61	35.26	0.29	0.00	0.00	99.27
KH03-21_1.1	27.32	4.68	32.79	33.87	0.30	0.00	0.00	98.96
KH03-21_1.2	28.45	1.71	33.15	36.13	0.29	0.00	0.00	99.74
KH03-21_1.2	26.90	4.61	33.12	35.02	0.30	0.00	0.00	99.95
KH03-21_1.3	31.95	1.84	32.41	31.81	0.33	0.00	0.00	98.34
KH03-21_1.3	8.79	0.12	37.50	51.19	0.17	0.00	0.00	97.78
KH03-21_2.1	16.27	0.28	37.32	45.54	0.32	0.01	0.00	99.74
KH03-21_2.2	23.86	0.20	37.12	38.23	0.28	0.02	0.00	99.71
KH03-21_2.2	2.69	22.59	34.17	38.63	0.09	0.00	0.00	98.17
KH03-21_3.1	16.26	0.51	36.61	44.66	0.32	0.00	0.00	98.36
KH03-21_3.2	28.27	2.23	32.06	34.91	0.30	0.00	0.08	97.85
KH03-21_3.2	21.26	9.25	32.34	35.15	0.24	0.00	0.00	98.24
KH03-21_4.1	10.86	0.53	36.61	51.03	0.29	0.00	0.02	99.34

KH03-21_4.1	28.43	0.32	33.99	37.41	0.63	0.00	0.00	100.77
KH03-22_A1	34.08	1.64	33.00	30.58	0.25	0.00	0.02	99.56
KH03-22_A3	17.17	0.62	37.28	44.37	0.27	0.00	0.00	99.71
KH03-22_A3	33.46	1.65	33.16	31.20	0.29	0.00	0.02	99.79
KH03-22_A3	29.88	4.26	34.10	32.16	0.28	0.00	0.00	100.68
KH03-22_A4	34.77	1.21	32.31	30.09	0.28	0.00	0.20	98.85
KH03-22_A4	17.75	0.39	37.76	43.64	0.28	0.00	0.00	99.81
KH03-22_A5	19.17	0.45	37.84	41.91	0.24	0.00	0.00	99.62
KH03-22_A5	36.16	0.95	33.10	28.58	0.29	0.00	0.09	99.17
KH03-22_A6	18.69	0.49	37.39	42.94	0.24	0.00	0.00	99.75
KH03-22_B1.1	14.38	0.32	37.28	45.47	0.20	0.00	0.00	97.65
KH03-22_B1.2	28.23	0.47	34.70	36.35	0.30	0.00	0.03	100.07
KH03-22_B1.3	16.13	0.30	38.29	44.18	0.25	0.00	0.06	99.22
KH03-22_B1.4	31.54	2.12	33.18	30.75	0.32	0.00	0.19	98.09
KH03-22_B1.4	12.55	0.41	38.17	48.15	0.23	0.02	0.03	99.57
KH03-22_B2	19.65	0.54	36.18	40.99	0.24	0.01	0.01	97.63
KH03-22_B3.1	31.93	1.59	33.02	31.86	0.32	0.00	0.02	98.74
KH03-22_B3.1	13.09	0.55	37.36	47.66	0.22	0.00	0.00	98.89
KH03-22_B3.2	34.07	1.11	32.71	30.02	0.30	0.00	0.00	98.21
KH03-22_B3.2	17.56	0.23	37.25	43.34	0.24	0.00	0.00	98.62
KH03-22_B4.2	16.95	0.46	36.98	43.82	0.27	0.01	0.07	98.57
KH03-22_B4.1	32.71	1.00	33.49	30.94	0.29	0.00	0.00	98.42
KH03-22_B4.1	19.94	0.56	37.44	40.68	0.28	0.00	0.00	98.91
KH03-23_A1	1.10	25.91	34.21	36.11	0.04	0.01	0.01	97.39

Table S4. Re–Os elemental abundance and isotope data for sulfides from KH03-15, KH03-16, KH03-21 and KH03-24 (modified after Harvey et al., 2011). Errors shown are 2 σ. Re and Os concentrations expressed as μg g^{-1}. For analytical standards and corrections for $^{18}O/^{16}O$ and $^{17}O/^{16}O$ refer to Table 2 of Harvey et al., (2011).

Sample	[Os]	[Re]	$^{187}Os/^{188}Os$	2 s.e.	$^{187}Re/^{188}Os$
KH03-15_2	0.001	0.848	0.2163	0.0073	3575
KH03-15_4	24.70	11.3	0.1195	0.0003	2.18
KH03-15_5	36.9	2.83	0.1208	0.0002	0.37
KH03-15_6	10.9	0.140	0.1202	0.0002	0.03
KH03-15_7	6.05	-	0.1304	0.0003	-
KH03-15_9	5.82	-	0.1185	0.0003	-
KH03-15_10	21.2	-	0.1312	0.0004	-
KH03-16_2	0.51	1.35	0.1349	0.0015	12.7
KH03-16_3	0.010	138.9	0.1424	0.0050	68722
KH03-16_4	1.48	34.27	0.1556	0.0051	111
KH03-16_5	12.9	0.294	0.1235	0.0001	0.11
KH03-16_6	0.024	3.133	0.1819	0.0057	622
KH03-16_9	1.74	-	0.1362	0.0010	-
KH03-16_10	0.052	-	0.3729	0.0169	-
KH03-21_1	0.992	1.252	0.1303	0.0006	6.02
KH03-21_2	1.11	1.181	0.1694	0.0004	5.11
KH03-21_3	2.72	0.056	0.1283	0.0003	0.098
KH03-21_4	10.0	23.32	0.1291	0.0001	101
KH03-21_5	9.97	-	0.1259	0.0008	-
KH03-21_6	1.29	-	0.1302	0.0008	-
KH03-21_7	0.843	-	0.1368	0.0008	-
KH03-21_8	4.48	-	0.1282	0.0005	-
KH03-21_9	0.447	-	0.1764	0.0012	-
KH03-21_10	0.584	-	0.1385	0.0005	-
KH03-24_5	1.69	0.01	0.1227	0.0004	0.020
KH03-24_10	0.195	0.002	0.1237	0.0028	0.050
KH03-24_11	0.231	-	0.1240	0.0006	-
KH03-24_14	2.76	0.04	0.1226	0.0013	0.070
KH03-24_15	2.54	35.87	0.1234	0.0004	67.4
KH03-24_16	2.50	18.78	0.1238	0.0011	35.8
KH03-24_17	0.600	27.27	0.1264	0.0005	217
KH03-24_20	0.314	-	0.1449	0.0017	-

Table S5. "Metasomatic" processes observed in the Kilbourne Hole peridotite xenoliths from this study. (i) Melt-rock interaction in antiquity; (ii) recent melt-rock interaction (a) spongey clinopyroxene rims, (b) observed interstitial glass; (iii) refertilization; (iv) cryptic metasomatism. Modified from Harvey et al. (2012).

"Metasomatic" process	(i)	(iia)	(iib)	(iii)	(v)
Group 1 peridotites					
KH03-2					
KH03-6					
KH03-7					
KH03-10		x			
KH03-11					
KH03-18					
KH03-25					
KH03-27		x			
KH96-2					
KH96-18					x
Group 2 peridotites					
KH03-3	x			x	x
KH03-15		x	x		
KH03-16			x		
KH03-21			x		x
KH03-24		x			
KH96-8	x				x
KH96-24					x